ESA Climate Change Initiative Plus
Soil Moisture

Product User Guide (PUG)

Supporting Product Version v06.1

Deliverable ID: D4.2 Version 2

16-04-2021

Prepared by

Earth Observation Data Centre for Water Resources Monitoring (EODC) GmbH

in cooperation with

TU Wien, VanderSat, CESBIO and ETH Zürich

This document forms the deliverable D4.2 Version 1, Product Users Guide (PUG) and was compiled for the European Space Agency (ESA) Climate Change Initiative Plus Soil Moisture Project (ESRIN Contract No: 4000126684/19/I-NB: ”ESA CCI+ Phase 1 New R&D on CCI ECVS Soil Moisture”).

For more information on the CCI programme of ESA see https://climate.esa.int/en/.

Number of pages: 72

Authors:		R. van der Schalie, W. Preimesberger, A. Pasik, T. Scanlon, R. Kidd	
Circulation:		ESA, Project Internal Public Release ONLY after review completed by ESA	
Issue	Date	Details	Editor
v1	29/05/2020	Update of document to support version 5.2 of the ESA CCI SM product. Included restructuring to a single document. Changes to he product included the addition of SMAP as well as updating the input data to LPRMv6 (PASSIVE and COMBINED) and the rescaling of AMSR2 to AMSRE (PASSIVE only). All products now use an updated CDF matching scheme. Temporal extent of product is to the end of 2019.	AP, RK, WP, WD, LM, TS
v2	08/02/2021	Update to reflect version 5.3 of the dataset which is a temporal extension to end of December 2020.	TS
v2.0,Issue 0.1	08/02/2021	Update to reflect version 6.1 of the dataset which is a major algorithmic development over v05.3. Updates include: increased time period used for TMI, cross flagging implemented for frozen soils and improved SNR-VOD regression by splitting into land cover classes. All input passive sensor data has been updated to LPRMv6.1 and a new experimental ASCAT dataset is used. Temporal extent of product is to the end of 2020. Within document, relevant text and diagrams updated. Section on known limitations removed as this is included within the ATBD for users. Some information has been moved to other sections to avoid repetition and all references are now collected in a single section.	TS
v2.0, Issue 0.2	02/03/2021	Reviewed. Updated ToC, updated formatting, To ESA for review	RK
v2.0, Issue 0.3	30/03/2021	Updated in line with reviewer comments. Changes to Section 4 on applications. Comments provided in revised RID document.	TS
V2.0 Issue 0.4	06/04/2021	Review. Updated header, accepted all changes prior to issue 0.2. To ESA for review	RK
V2.0 Issue 1.0	16/04/2021	Finalised	RK

For any clarifications please contact Richard Kidd (richard.kidd@eodc.eu).

Project Partners

Prime Contractor and project management	**EODC,** Earth Observation Data Centre for Water Resources Monitoring (Austria)
Earth Observation Partners	**TU Wien**, Vienna University of Technology (Austria) **VanderSat**, The Netherlands **CESBIO**, France
Climate Research Partners	**ETH**, Institute for Atmospheric and Climate Science, (Switzerland)

Table of Contents

List of Figures

List of Tables

Definitions, acronyms and abbreviations

Acronym	**Full Name**
AMI-WS	Active Microwave Instrument - Windscat (ERS-1 & 2)
AMSR-E	Advanced Microwave Scanning Radiometer-Earth Observing System
ASCAT	Advanced Scatterometer (Metop)
ATBD	Algorithm Theoretical Basis Document
CCI	Climate Change Initiative
CECR	Comprehensive Error Characterization Report
DARD	Data Access Requirement Document
DMSP	Defense Meteorological Satellite Program
DPM	Data Processing Model
EASE	Equal-Area Scalable Earth
ECV	Essential Climate Variable
ERA-Interim	ECMWF Reanalysis Interim
ERA-Land	ECMWF Reanalysis land water resources dataset
ERS	European Remote Sensing Satellite (ESA)
ESA	European Space Agency
EUMETSAT	European Organisation for the Exploitation of Meteorological Satellites
FTP	File Transfer Protocol
GCOS	Global Climate Observing System
GLDAS	Global Land Data Assimilation System
IODD	Input Output Data Description
ISEA	Icosahedron Snyder Equal Area
ISEA4H	Icosahedron Snyder Equal Area (ISEA) Aperture 4 Hexagonal
JAXA	Dokuritsu-gyosei-hojin Uchu Koku Kenkyu Kaihatsu Kiko, (Japan Aerospace Exploration Agency)
JULES	Joint UK Land Environment Simulator
LDAS	Land Data Assimilation System
MERRA	Modern-Era Retrospective Analysis for Research and Applications
METOP	Meteorological Operational Satellite (EUMETSAT)
MIRAS	Microwave Imaging Radiometer using Aperture Synthesis
NaN	Not A Number
NASA	National Aeronautics and Space Administration
NetCDF	Network Common Data Form

NWP	Numerical Weather Prediction
PDF	Probability Distribution Function
PSD	Product Specification Document
PUG	Product User Guide
RFI	Radio Frequency Interference
SAR	Synthetic Aperture Radar
SM	Soil Moisture
SMMR	Scanning Multichannel Microwave Radiometer
SMOS	Soil Moisture and Ocean Salinity
SRD	System Requirements Document
SSD	System Specification Document
SSM	Surface Soil Moisture
SSM/I	Special Sensor Microwave Imager
SURFEX	SURFace EXternalized module
SWI	Soil Water Index
TBD	to be determined
TMI	TRMM Microwave Imager
TRMM	Tropical Rainfall Measuring Mission
UTC	Coordinated Universal Time

Executive Summary

The ESA CCI SM v06.1 product consists of three surface soil moisture data sets: The “ACTIVE Product” and the “PASSIVE Product” were created by fusing scatterometer and radiometer soil moisture products, respectively; The “COMBINED Product” is a blended product based on the former two data sets. Data files are provided as NetCDF-4 classic format and comprise global merged surface soil moisture datasets at daily temporal resolution. The data set spans over 40 years covering the period from November 1978 to December 31st 2020.

The theoretical and algorithmic basis of the product is described in the Algorithm Theoretical Basis Document (ATBD) for ESA CCI SM v06.1 (Scanlon et al. ,2021), and reported by Wagner et al. (2012). The SNR (signal-to-noise-ratio) merging algorithm introduced for the first time in version 3.2 is described in Gruber et al. (2017), and later updated in Gruber et al. (2019), and include an overview of the errors of the soil moisture datasets for those version numbers. Further documentation relating to the product, and reference documents are provided in Section **Error! Reference source not found.** and can be found on the CCI Soil Moisture project web site (http://www.esa-soilmoisture-cci.org).

The location and full access details to the product are provided to users after completion and verification of a user registration form. Users can either register to access the product from the User Registration form on the CCI Soil Moisture Website, or can directly access the product, without requirement for registration from ESA’s CCI Open Data Portal[1].

The product is provided in a format that currently complies with the minimum standard format requirements as detailed by the CCI data standards working group (DSWG) (Bennet and James, 2013). For this reason ESA CCI SM v06.1 is provided in NetCDF-4 classic format and is also compliant with the NetCDF Climate and Forecasting group best practice[2] (Eaton et al., 2017).

The ACTIVE product of ESA CCI SM (consisting of soil moisture from the ERS and ASCAT sensors) uses the latest available version of the H SAF ASCAT SSM product (HSAF 2018). Improvement of the ACTIVE product of ESA CCI SM is therefore largely dependent from developments carried out by H SAF. Descriptions of ASCAT Soil Moisture in this document are just to highlight the differences between Scatterometer/Radiometer derived soil moisture products and should help the users of ESA CCI SM understand which products fits best for their purpose.

---

[1] http://cci.esa.int/data

[2] http://cf-pcmdi.llnl.gov/documents/cf-conventions/latest-cf-conventions-document-1

1 Introduction

The purpose of the Product User Guide (PUG), intended for users of the ESA CCI soil moisture product, is to describe the ECV data product with a focus on:

- the geophysical data product content
- the product flags and metadata
- the data format
- the product grid and geographic projection
- how people use the product and the tools available

Since the users of the soil moisture product come from a wide and varied audience, with differing levels of knowledge in the field of retrieval of soil moisture information from satellite observations, this document provides some relevant background aiming to enable a common understanding (further information is available in the ATBD for v06.1, Scanlon et al., 2021). Section 4 provides an overview of the pivotal role that soil moisture plays within the environment and section 5 provides an overview of its retrieval from earth observation satellites.

Section 6 is largely taken from (Dorigo et al., 2017) and it presents the broadest review, to date, of the current use and application of the ESA CCI SM product by the wider scientific community. In this section it is shown how ESA CCI SM has contributed to improved process understanding in the following Earth system domains: climate variability and change, land-atmosphere interactions, global biogeochemical cycles, hydrological and land surface modelling, drought applications, and meteorology.

Section 7 provides details of the product characteristics including the geophysical parameters that are available in the products, their respective data volumes, and the physical structure and format of the product and associated quality flags and indicators.

In Section 8 the opportunity is taken to provide an overview of key points relating to data access, team contact, and restates the acknowledgement to be cited in the use of the ECV SM products.

For reference, Section 9 provides definitions of some common terminology used within the earth observation domain and the bibliography is provided in Section 10.

2 Soil Moisture within the environment

The central role of soil moisture for the environment is well known. Its contribution e.g. to hydrological and agricultural processes, linked to e.g. runoff generation, drought development, and irrigation, respectively, is evident. Moreover, it significantly impacts the climate system through feedbacks to the atmosphere. As a source of water for evapotranspiration over the continents, soil moisture is involved not only in the water but also in the energy cycle. Approximately 60% of precipitation over land is returned to the atmosphere as evapotranspiration (Oki and Kanae 2006), and this flux also uses up more than 50% of all net radiation over land (Dirmeyer et al. 2006). The investigations of possible effects of soil moisture on the climate date back to the 70s and 80s (Shukla and Mintz 1982). In the recent years soil moisture-climate interactions received an increasing attention (Seneviratne et al. 2010). Moreover, in 2004 soil moisture was recognised as an essential climate variable (ECV) and finally added in 2010 to the list of terrestrial ECV by the Global Climate Observation System (GCOS).

A number of numerical experiments have established the sensitivity of atmospheric fields to soil moisture dynamics (Diffenbaugh et al. 2007; Fischer et al. 2007a; Jaeger and Seneviratne 2011; Koster et al. 2004a; Seneviratne et al. 2006b). On short time scales, which are relevant for numerical weather prediction, soil moisture variations seem to have a more significant influence on the surface energy budget and on the planetary boundary layer structure than changes in other terrestrial variables such as roughness or albedo (Mahfouf 1991). The importance of soil moisture for sub-seasonal and seasonal forecasting is also well established (Koster et al. 2004a; Koster et al. 2010), and is additionally impacted by the memory associated with soil moisture (Entin et al. 2000; Seneviratne et al. 2006b; Vinnikov et al. 1996; Wu and Dickinson 2004).

Most of the impacts of soil moisture on the climate system are induced by its coupling to evapotranspiration, and resulting impacts on temperature and precipitation (Seneviratne et al. 2010). Strongest feedbacks between land and atmosphere are expected in regions with soil moisture-limited evapotranspiration regimes, given by the control of soil moisture on evapotranspiration (Hirschi et al. 2011). Mostly affected are transitional zones located between wet and dry climates (Koster et al. 2004a; Seneviratne et al. 2006b), where soil moisture is limiting for evapotranspiration and can strongly vary on both intra-annual and inter-annual time scales. This coupling has been shown to be of strong relevance for climate variability in mid-latitude regions, in particular for the occurrence of heat waves (Fischer et al. 2007c). Impacts on precipitation are less consistent across studies, but are found to include a number of direct and indirect feedbacks (Findell and Eltahir 2003). In the context of climate change, regions with transitional climate regimes are expected to be shifted poleward, with a possible increase in climate variability induced by soil moisture feedbacks in regions with currently wet climate regimes. Supporting numerical studies, recent observational studies have shown evidence for soil moisture impacts on hot extremes (Hirschi et al. 2011) as well as global evapotranspiration (Jung et al. 2010).

Furthermore, it is possible that soil moisture anomalies may also affect large-scale circulation patterns. For the United States, the study of Pal and Eltahir (2003) has suggested that soil moisture anomalies over relatively small regions may induce floods and droughts not only locally, but also over distant areas. A relationship between the depletion of early summer soil moisture and the development of heat lows over the Mediterranean region in late summer has also been noticed in Haarmsa et al. (2009).

A factor influencing soil moisture-climate interaction is the vegetation. Transpiration is the evaporation through the plant stomata, which is regulated by several factors including soil moisture. Therefore, land cover and its variation in time are expected to play a crucial role for soil moisture-climate interactions. A possible impact of vegetation cover during the European heat wave 2003 was shown in Zaitchik et al. (2006) by comparing temperature anomalies over pastures and forests, showing higher heat anomalies over the pastures during the August peak of the 2003 European summer drought and heat wave. The study by Teuling et al. (2010), based on measurements from the Fluxnet network, also identified differences in the energy fluxes over grassland and forest sites during heat wave days, although the results were in partial contrast to those of Zaitchick et al. (2006). For typical heat wave days, it was found that the forest led to a higher warming of the atmosphere than grassland, because the former used less energy for evapotranspiration than the latter. However, the implications are that in the long term the soil moisture depletion over grassland is faster than over forest, and consequently grassland would lead to higher warming after long dry and hot periods. This study highlighted the time-scale dependence of feedbacks between land surface processes and the climate, and its strong relation to soil moisture dynamics.

All of the mentioned feedbacks and interactions are particularly relevant for drought development, and especially agricultural (or soil moisture) drought. This is another area where the increasing availability of soil moisture observations can help investigate and diagnose the underlying driving processes, e.g. the respective role of large-scale circulation patterns versus land-atmosphere feedbacks for drought development (Rowell and Jones 2006; Schubert et al. 2004).

3 Soil Moisture Data from Earth Observation Satellites

This section provides a general overview of the different types of data and the methods, technologies and processes employed to generate the Soil Moisture Data Products from the measurement to their application/analysis.

3.1 Microwave Instruments onboard Earth Observation Satellites

There are two principal types of remote sensing, corresponding to the following types of microwave instruments: (a) scatterometers and radars which measure the radar backscattering coefficient σ^0 in physical units [dB] or [m^2/m^2], and (b) radiometers which measure the brightness temperature T_B in physical unit [K]. Instruments in group (a) are called *active* because they use their sown source of electromagnetic energy for the measurement, while the ones in group (b) are referred to as *passive* instruments because they measure energy that is reflected or emitted from the earth surface.

Figure 1 identifies the active (at the bottom) and the passive (at the top) microwave instruments that are used for the production of the Soil Moisture ECV Data Products, their hosting satellites, and their times of operation.

- AMI-WS and ASCAT are (active) C-band scatterometer instruments onboard the ERS and METOP satellites, respectively. Note that AMI-WS is still labelled “SCAT” in the picture, though the former name is nowadays preferred.
- SMMR, SSM/I, TMI, AMSR-E, AMSR-2, MIRAS, SMAP L-band Radiometer, GMI, MWRI and WindSat are (passive) multi-frequency radiometer instruments onboard the Nimbus-7, DMSP, TRMM, Aqua, GCOM-W1, SMOS, SMAP, GPM, FY-3B and Coriolis satellites, respectively.

These instruments are characterized by their high suitability for Soil Moisture retrieval and their technological maturity.

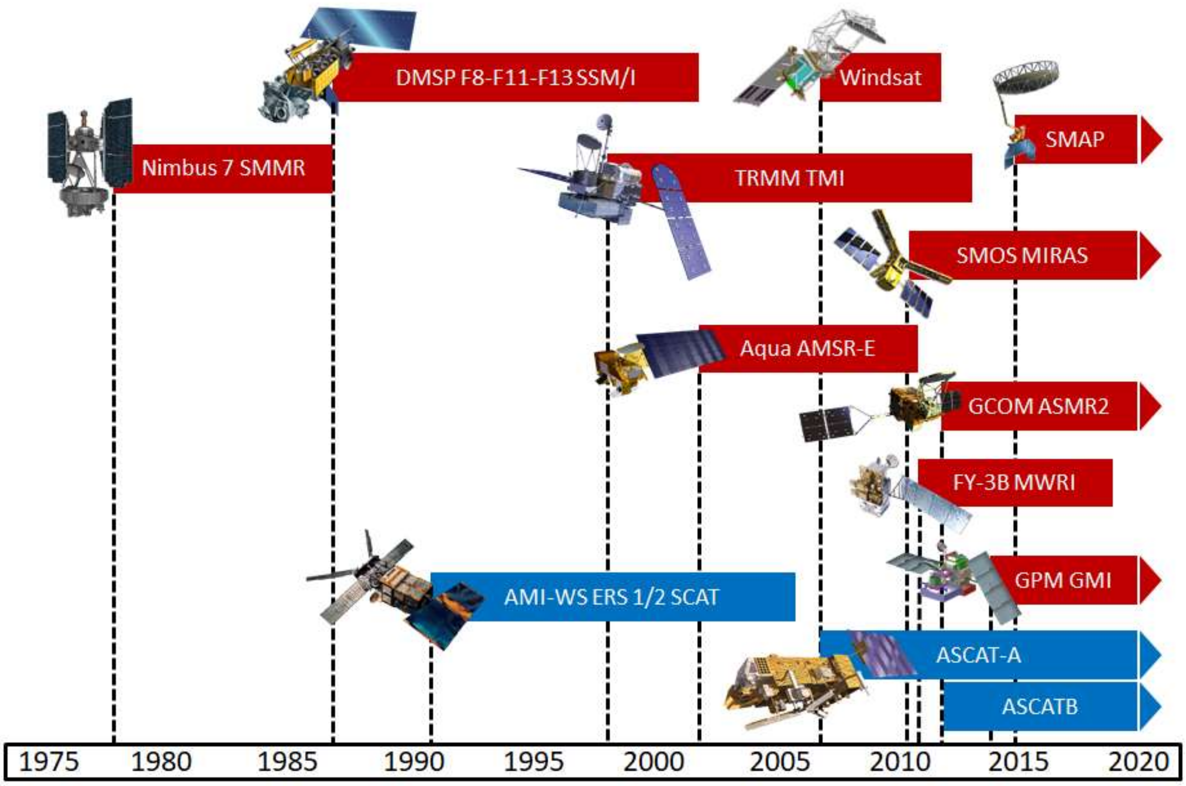

Figure 1: Microwave Instruments used for the generation of Soil Moisture ECV Data Products (version 06.1)

The ESA CCI SM processing system is designed to allow the integration of new instruments during its operational use phase. Since the initial product, many different satellite products have been added including SMAP, GPM and FY-3B.

In a single overpass (one orbit around the Earth) the satellite's instrument observes a wide swath of the land surface of a width somewhere between 500 to 1400 km. Satellite swath data is made of individual nodes (syn. pixels), each node being a measurement of either backscattering coefficient σ^0 (active) or brightness temperature T_B (passive) from an area (footprint) of 10-50 km diameter on the Earth surface.

Figure 2 shows the geometry of the wide swath imaging measurements made by AMI-WS (SCAT) and ASCAT instruments onboard the ERS and METOP satellites. The AMI-WS scatterometer (left part of Figure 2) consists of three antennae producing three beams looking 45° forward, sideways (90°), and 45° backward with respect to the satellite's motion direction along the orbit. The measurements from each beam consist of 19 nodes spaced 25 km apart. As the satellite beams sweep along the Earth surface yielding an approximately

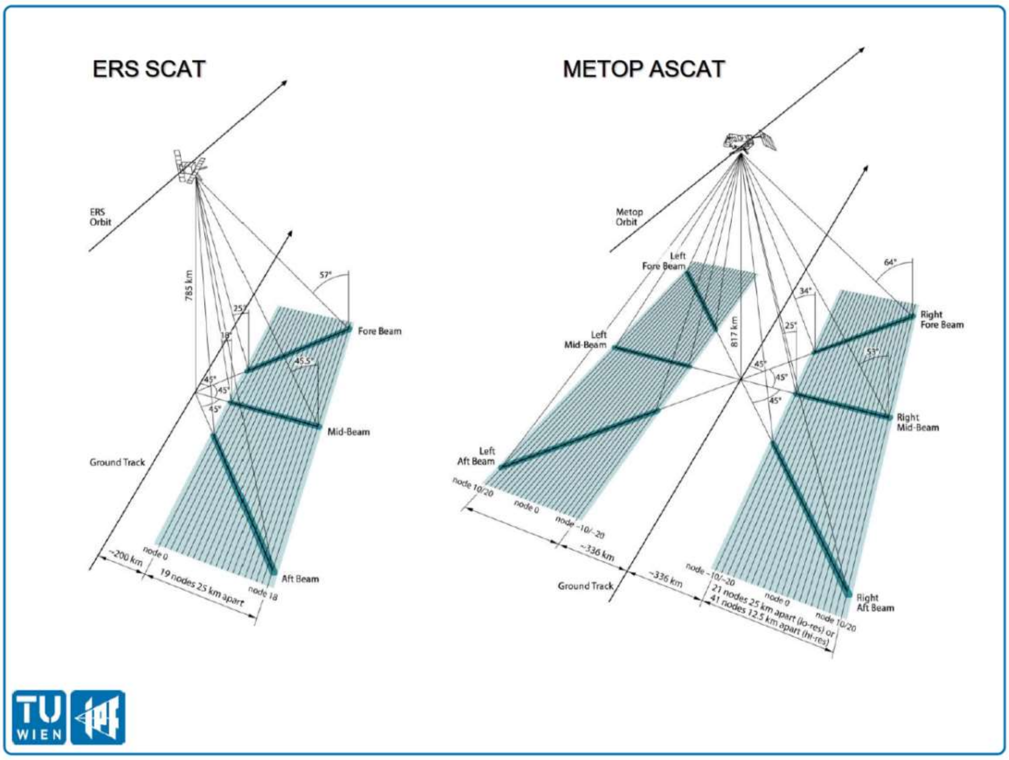

Figure 2: Beams and Wide Swaths of AMI-WS and ASCAT Instruments

500 km wide swath, each node produces its own σ^0 backscatter measurement, integrated over an area around 50 km in diameter. The three measurements originating from the three beams during the single satellite overpass are called triplets.

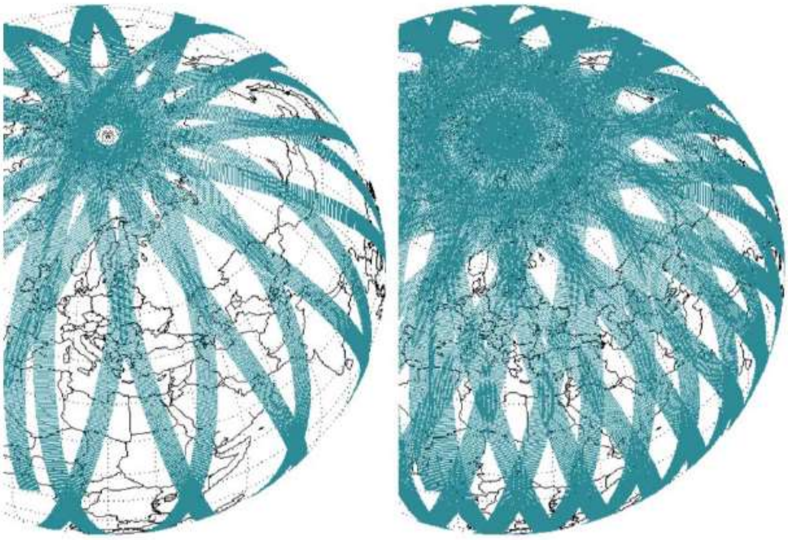

Figure 3: Wide Swaths and Daily Global Coverage of AMI-WS (left) and ASCAT (right)

The ASCAT scatterometer (right part of Figure 2) is similar but consists of three antennae on either side, producing six beams. The measurements from each beam consists of 21 nodes spaced 25 km apart (lo-res) or 41 notes spaced 12.5 km apart (hi-res). While the satellite beams sweep along the earth surface a wide swath is observed on either side.

Figure 3 shows the orbits made by a single ERS satellite (left) and a single METOP satellite (right) and the wide swaths captured by AMI-WS and ASCAT instruments, respectively, during one day of observation time. The wide swaths of ASCAT have near-global revisiting times of 2–3 days.

Development of soil moisture retrieval algorithms from active MRS sensors is not part of the ESA CCI SM project. The latest available H SAF ASCAT SSM CDRs are used as input in ESA CCI SM. For a detailed description and the latest available products visit http://hsaf.meteoam.it/.

3.2 Data Processing Chain

The payload data received from a satellite passes through a chain of processing which has the following principal steps:

- Level 0: Reconstructing the raw instrument data from a satellite's payload data transmissions received at satellite ground stations, and archiving them at a data centre.
- Level 1: Converting the raw instrument data of a single overpass swath to calibrated measurements (observations) of radar backscattering coefficient σ^0 in [dB] or [m^2/m^2] (in case of active instrument), or brightness temperature T_B in [K] (in case of passive instrument).
- Level 2: Retrieving the Surface Soil Moisture (SSM) geophysical parameter – in physical units [%] or [m^3/m^3] – from the calibrated measurements of a single overpass swath.
- Level 3: Generating the consistent and global Soil Moisture ECV Data Products by merging the SSM time series acquired from many satellites over many years – this is the objective of the system specified herein.
- Level 4: Analysing the lower level data to determine the state or change of state (events, processes) of regional or global climate systems.

The following section provides a brief survey of the different processing levels tailored to Soil Moisture. There is also a fine-grained organization within the levels, in terms of sublevels or product categories, but these are suppressed in the first survey. A full specification of data processing levels is available in IODD (Kidd et al., 2013).

Levels 0-1:

The steps up to Level 1, from the instrument to the calibrated measurement result, follow the principles of measurement as outlined in (JCGM 2008), and (JCGM 2012). Note that a measurement (syn. observation) is not necessarily made with a single antenna, instrument, or even a single satellite. Crucial is that the individual measurement devices contributing to the measurement result are synchronized (with sufficient accuracy in space and time) to the spatial-temporal coherency characteristics of the observed source. Therefore, the calibrated measurement may be summed from many antennas (e.g. in case of the SMOS MIRAS instrument, which uses aperture synthesis) or even summed from satellites in formation flying. In any case, because the observations made at different orbits do not satisfy the coherency criteria, Level 1 data are observations from a single overpass.

Levels 2-3:

The situation changes for the Levels 2 and 3, which are about the art of estimating values of quantities that cannot be directly measured with remote sensing instruments. The mathematical-physical basis for this process is that there is a functional relation between object parameters X and instrument observables Y. Symbolically, the relation may be written as $Y = f(X)$ (forward model) or $X = g(Y)$ (inversion). It is known that at any time object parameters X and observables Y have definite values. Once sufficient information is obtained from measurements of Y, estimates of X can be determined under certain conditions, if there is sufficient knowledge of a suitable model or inversion. To indicate this radical difference, this process is no longer called measurement but “retrieval”.

In the case of the ECV Production System the observed object is an area of the top soil surface layer (of approx. 25x25 km size and < 2 cm thickness), and the retrieved geophysical parameter is Soil Moisture, expressed in the physical unit [%] or $[m^3/m^3]$.

Depending if the measurement was made with an active or a passive microwave instrument, respectively, either a change detection approach or a forward modelling method is utilized. Both methods, like geophysical parameter retrieval in general, require use of additional ancillary data, which can be long-term reference data (historical data, climate data) or model parameters.

Levels 2 and 3 have in common that the retrieved parameters are local state variables: they characterize the state of a local and compact object in space (i.e. a local physical system), at a moment or period in time. They are thus distributions in space (over the land surface in case of Soil Moisture) and time. The difference between Level 2 and 3 is that the parameter retrieved by a process of Level 2 adheres to the locality condition of a single Level 1 measurement, while this condition is relaxed at Level 3. In practice, Level 3 is about merging Level 2 data from different observation times, orbits or instruments.

For full descriptions of the retrieval and merging methods cf. ATBD for v06.1 (Scanlon et al., 2021) and (Wagner 2012).

Level 4:

At Level 4 analyses of data from Levels 3, 2 or 1 are performed in order to determine the state or the change of state of specific geo-physical systems of interest, in particular regional and global climate systems. Detection of change of state typically involves statistical analysis methods (e.g. trend analysis) and process model calculations (simulations) using lower level data as input.

Present at all Levels of the data processing chain (but omitted in the discussion so far) are processes to determine measures for the degree of uncertainty associated with the resulting data. At Levels 0 and 1 an adequate measure is the measurement uncertainty as described e.g. in (JCGM 2008), and at Levels 2 and 3 the error characterization as described in the E3UB (Scanlon et al. 2020). We do not know what measures are used at Level 4 but we note that results of analyses and simulations may be in the range of evidentiary to indicative.

3.3 Grid Types

The data acquired by a satellite instrument constitute individual measurements per swath node (actually one measurement result per beam, overpass and swath node) and are spatially arranged in the geometry of a *swath grid*, as illustrated in Figure 2. Swath grids are dynamical (with respect to the Earth surface) because they are a projection made by the moving satellite. The Level 0 data are necessarily raster data from a swath grid. Typically, Level 1 and 2 data provided by ESA, EUMETSAT, NASA and JAXA are still in the geometry of swath grids, and annotated with time- and geo-referencing information to allow inference of time and geo-location of each swath node. Data in swath grid geometry are usually distributed as one raster per half-orbit i.e. one raster for the ascending orbit direction and a second raster for the descending orbit direction. The format of geo-referencing information varies; it may be given per raster as a whole or even as (latitude, longitude) coordinates per grid node.

Technically, it can be of advantage to map the swath grid nodes, onto a (spatial) *global grid*[3] which is uniformly and statically covering the Earth surface. Cases where mapping to a global grid is already performed at Level 1 are Nimbus-7 SSMR, DMSP SSM/I and SMOS MIRAS, and at Level 2 METOP ASCAT. Note that a global grid maps the space dimensions only, while time-referencing annotation is still maintained for the individual measurements.

Figure 4 shows the equally spaced, equal area WARP 5 global grid used for the ASCAT Level 2 SSM. The principle of construction (indicated in the upper part of Figure 4) is as follows: a) create equally spaced latitude small circles at distances *a*, and b) on each latitude circle create grid points at discrete longitudes, again with a fixed spacing of *a*. Due to the construction the

---

[3] The technical term is Discrete Global Grid (DGG), however, as we do not know how a non-discrete (i.e. continuous) grid would look like, we do not use this term herein.

global grid has areas with irregularities. The lower part of Figure 4 shows: a) the regularity at origin, b) the divergence at the North Pole, and c) the dislocation at the 180° meridian.

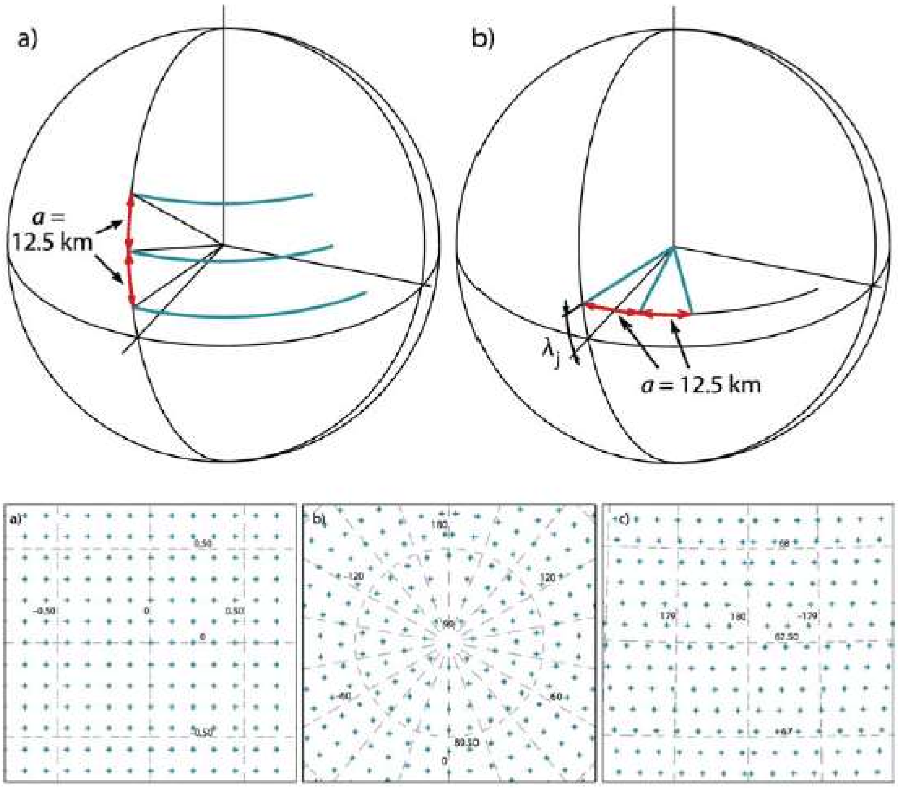

Figure 4: Construction of the WARP 5 Global Grid used for ASCAT L2 Data

Figure 5 a) shows the geodesic grid used for the SMOS Level 1 and Level 2 data, known as Icosahedron Snyder Equal Area (ISEA) Aperture 4 Hexagonal (ISEA4H) global grid. This grid is constructed by a subdivision method. Creating the grid involves subdividing the 20 equilateral triangles forming the faces of the regular icosahedron into more triangles, yielding 20 hexagons and 12 pentagons on the surface of the sphere (the so-called resolution 1 grid). Higher resolution grids are formed iteratively by tessellating the obtained shapes.

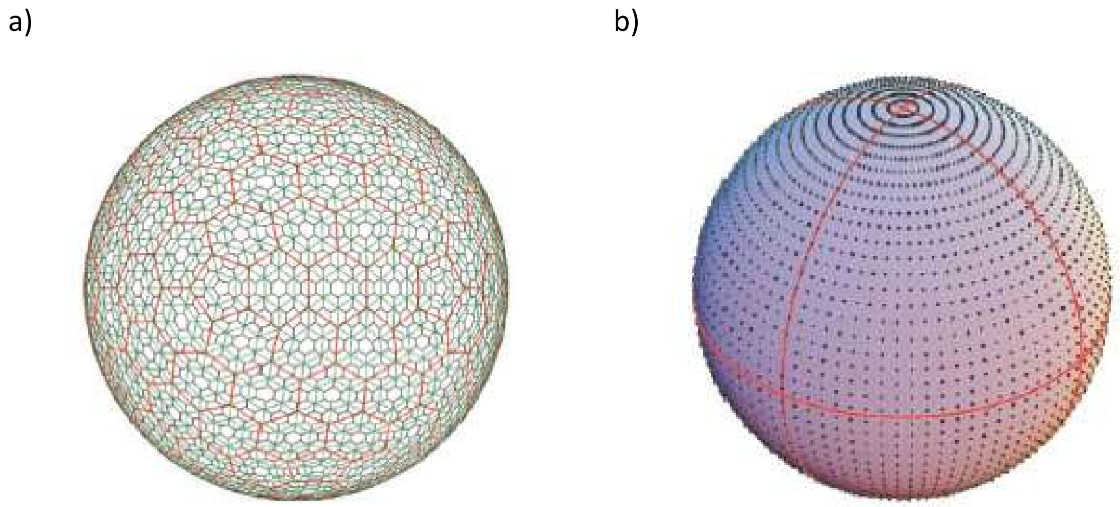

Figure 5: a) Geodesic ISEA4H grid of SMOS; b) regular latitude-longitude grid used for SM ECV

Figure 5 b) shows a regular latitude-longitude grid. Grid points are equally spaced in the latitude-longitude coordinate system, however, as can be readily seen in Figure 5, they are not equally spaced / equal area on the earth surface. This grid type is utilized for the Soil Moisture ECV Data Products.

Still for technical reason, it can be of advantage to proceed further and to map the value distributions onto a *global space-time grid*. This happens usually at Level 3 because it facilitates combining data from many orbits and satellites. Satellite data mapped to a space-time grid can be viewed in two ways: For a given time index we have a raster image that can be projected to and visualized on a geographic map; for a given spatial grid point we have a time series that can be visualized as a graph.

Table 1: Grid Systems used for Calibrated Measurement Data and SSM Geophysical Parameter Data

		Active		**Passive**						
		ERS AMI-WS	**METOP ASCAT**	**Nimb.7 SMMR**	**DMSP SSM/I**	**TRMM TMI**	**Aqua AMSR-E**	**Coriolis WindSat**	**SMOS MIRAS**	**GCOM-W1 AMSR-2**
σ^0/T_B	**L1**	swath	swath	EASE	EASE	swath	swath	swath	ISEA4H	swath
SSM	**L2**	WARP5	WARP5	lat-lon	lat-lon	swath	swath	swath	EASE2	swath

Table 1 lists the grid types used for the Level 1 calibrated measurements of radar backscattering coefficient σ^0 and brightness temperature T_B, and the SSM geophysical parameter data.

In the process of generating the Level 3 Soil Moisture ECV Data Products, the SSM geo-parameter data available in the different grid types are converted into a common space-time grid: a latitude-longitude grid (spatial resampling) and a reference time of 0:00 UTC (temporal resampling). This is the first step to produce a merged and harmonized ECV Data Product on a global and uniform space-time grid with a spatial resolution of 0.25 degree and a temporal resolution of one day.

A web-based tool to visualize and search for grid point information (e.g. geo-location, grid index, surface type) is available here: https://dgg.geo.tuwien.ac.at/

For more information about global grid systems cf. (Kidd 2005) and (Bartalis 2009).

3.4 ESA CCI SM Algorithm

The overall setup of systems follows a modular design to make best use of existing European and international services, and to ensure that new satellites and instruments can be integrated. All products integrated into the ESA CCI SM product are Level 2 SM products, further details of which can be found in the ATBD for v06.1 (Scanlon et al., 2021).

In summary, the major processing steps to product the ESA CCI SM product are (also shown in **Error! Reference source not found.**):

1. Spatial resampling and temporal resampling (including flagging and cross-flagging of observations)
2. Rescaling passive and active level 2 observations into radiometer and scatterometer climatologies (for the ACTIVE and PASSIVE product), and separately rescaling all level 2 observations into a common model-based climatology (for the COMBINED product)
3. Triple collocation analysis (TCA)-based error characterisation of all rescaled level 2 products
4. Polynomial regression between VOD and error estimates to fill spatial gaps where errors could not be reliably retrieved i.e., where TCA is deemed unreliable
5. Merging rescaled passive and active time series into the PASSIVE, ACTIVE, and COMBINED products, respectively.

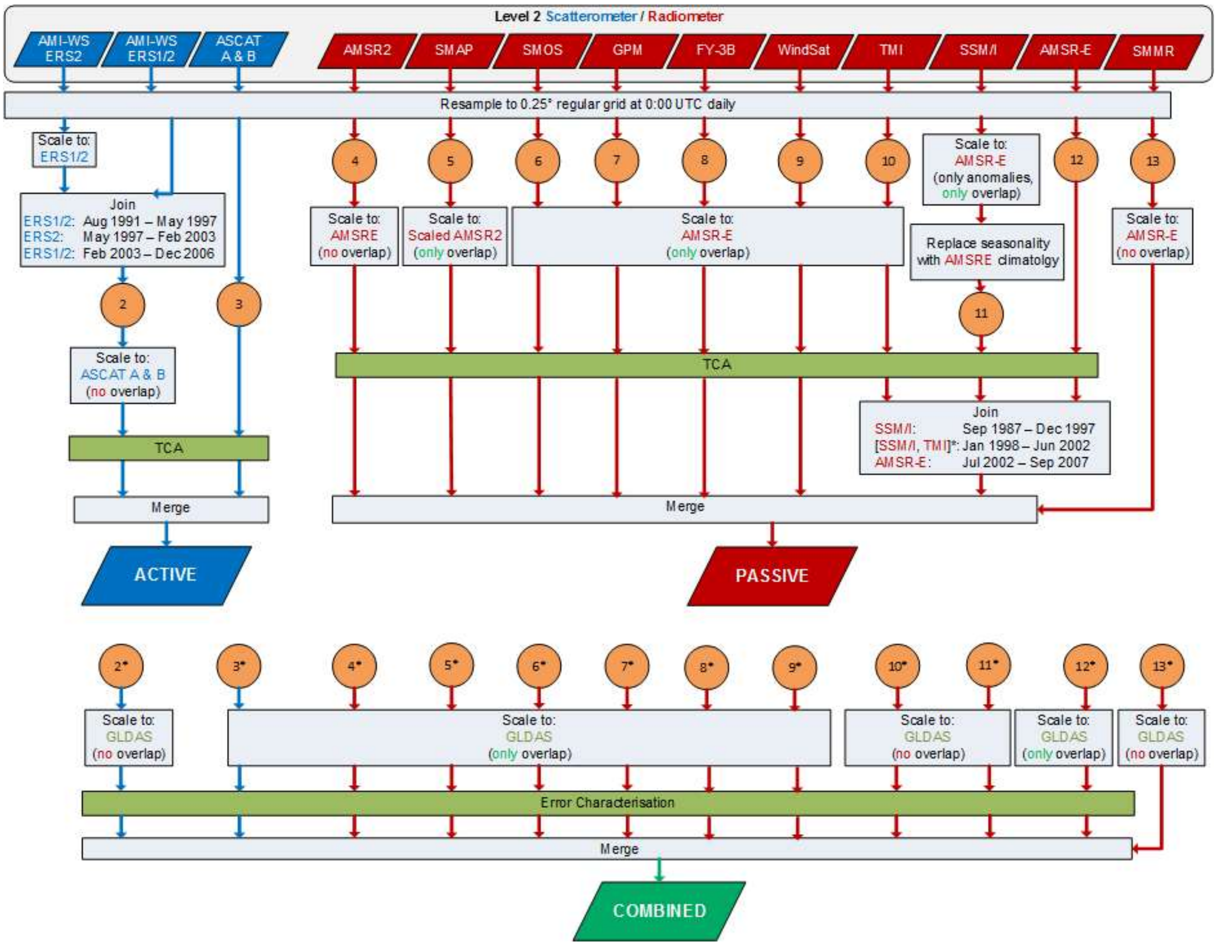

Figure 6: Principle Data Flow for the generation of Soil Moisture ECV Data Products, an overview of the processing steps in the ESA CCI SM product generation (v06.1). For more information see the ATBD.

3.5 Soil Moisture Data Products

As an example of a Soil Moisture product, Figure 7 shows the Soil Moisture anomaly for July 2020 derived from the ESA CCI SM v06.1 COMBINED product. The image shows the anomaly derived from an historical data record that combines measurements of multiple satellite instruments over the period 1979 to 2020. The reference period used for the anomaly calculation is 1991-2010. As this is based on soil moisture retrievals from passive microwave radiometry, the values are in m^3m^{-3}.

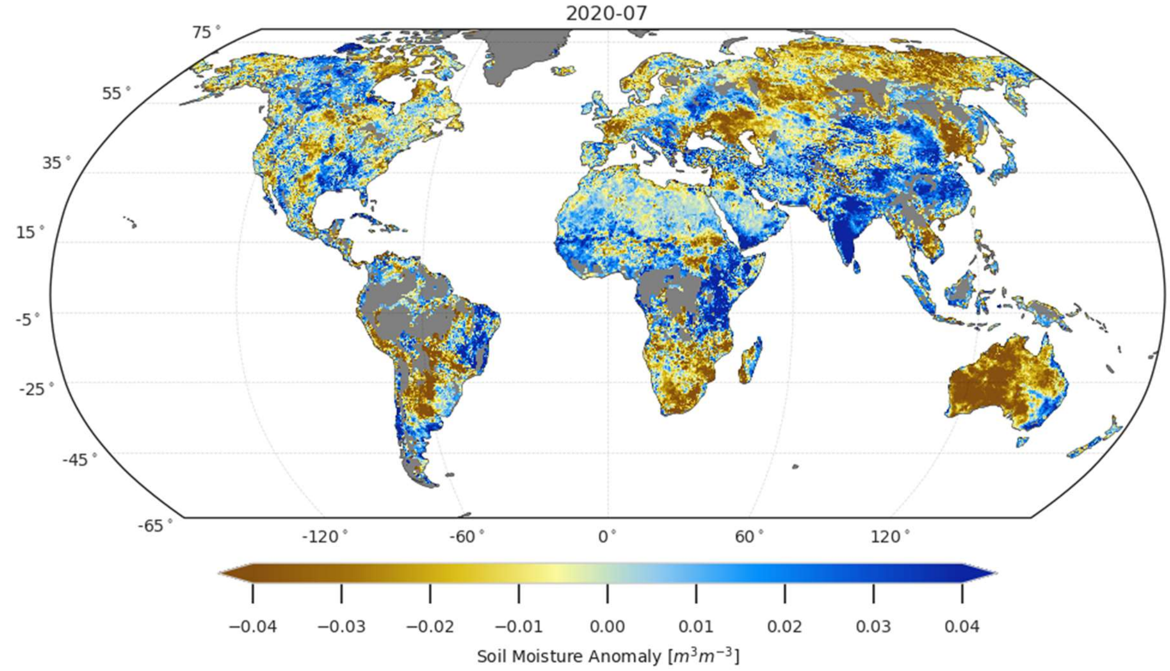

Figure 7: Soil Moisture Anomaly for July 2020 for the ESA CCI SM v06.1 COMBINED product (reference period: 1991-2010).

Surface Soil Moisture (SSM) parameter data from ERS AMI-WS and METOP ASCAT are an example of a Level 2 data product. It is retrieved from calibrated measurements of an active microwave instrument using the change detection method of TUW (ERS) and the further developed implementation by H SAF. The method relies upon the multi-incidence observation capabilities of the ERS and METOP scatterometers to model the effects of vegetation phenology. The SSM values of Active soil moisture retrievals are scaled between 0 and 1, representing zero Soil Moisture and saturation respectively. Parameter retrieval is not possible over tropical forest which affects about 6.5% of the land surface area.

Soil Water Index (SWI) parameter data are an example of a Level 3 data product. SWI is a measure of the profile Soil Moisture content obtained by filtering the SSM time series with e.g. an exponential function. Other typical examples of Level 3 products are the estimates of the Soil Moisture content for different soil layers and different temporal and spatial sampling characteristics, tailored to the needs of specific user groups.

4 ESA CCI SM in Earth system applications

The ESA CCI SM product is utilised in a variety of applications including climate modelling, hydrology and NWP systems. A detailed discussion of the applications up until 2017 is presented in Dorigo et al. (2017). This section provides information from that publication, highlighting key papers across a broad range applications. A summary of the number of papers published since 2017 for each application area is provided in Figure 8.

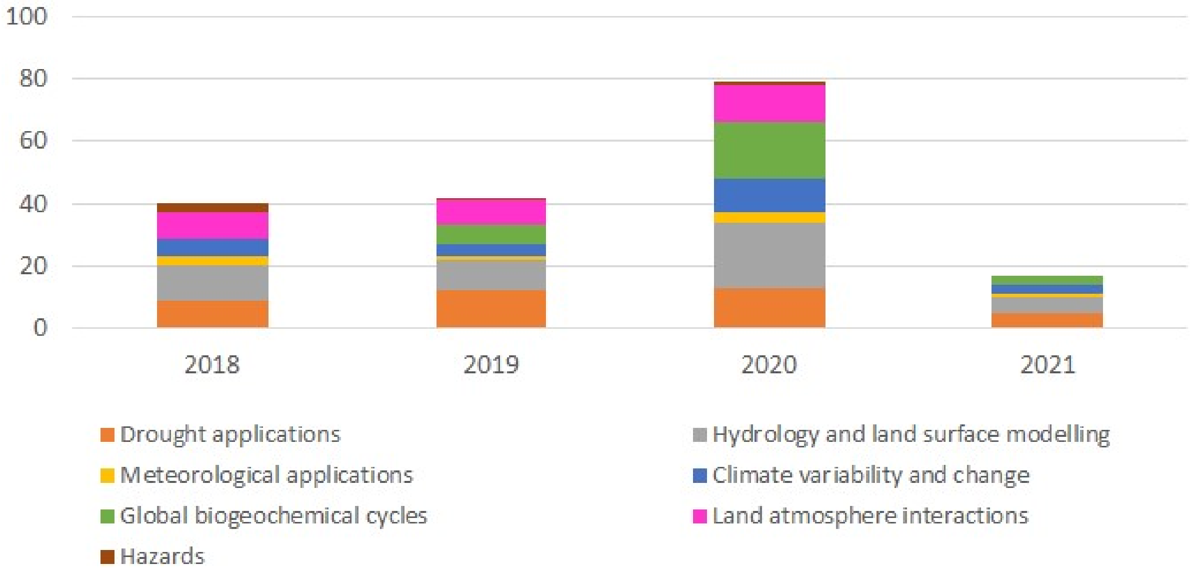

Figure 8: Papers by application area which use ESA CCI SM within their assessment over time (as of March 2021).

The following section is taken from (Dorigo et al. 2017) as is presents the broadest review to date of the current use and application of the ESA CCI SM product by the wider scientific community.

The use of ESA CCI SM products in a wide variety of studies helps improve our understanding of Earth system processes (**Error! Reference source not found.**), in particular with respect to climate variability and change. Even though the application fields are seemingly different, in all of them ESA CCI SM plays a central role in benchmarking, calibrating, or providing an alternative to the land surface hydrology in dedicated models. The following sections will provide an extensive synthesis of how ESA CCI SM has been used so far in the different application areas and what potential still remains unexploited.

Table 2: Applications where ESA CCI SM has been used to improve our Earth system understanding. Modified from Dorigo and De Jeu (2016).

Application area	**Main purpose**	**References**
Climate variability and change	Long-term trends in soil moisture	(Albergel et al. 2013; An et al. 2016; Dorigo et al. 2012; Qiu et al. 2016b; Rahmani et al. 2016; Su et al. 2016)
	Assessment of drivers of soil moisture trends	(Feng 2016; Liu et al. 2015)
	Soil moisture as driver of multi-annual variability in land evaporation	(Miralles et al. 2014b)
	Impact of ocean atmosphere system on soil moisture variability	(Bauer-Marschallinger et al. 2013; Miralles et al. 2014b; Nicolai-Shaw et al. 2016)
	Soil moisture as indicator of global climate variability and change	(De Jeu et al. 2011; De Jeu et al. 2012; Dorigo et al. 2014; Dorigo et al. 2015a; Dorigo et al. 2016; Parinussa et al. 2013)
	Impact of soil moisture trends on atmospheric composition	(Klingmüller et al. 2016)
	Validation of climate model runs	(Du et al. 2016; Lauer et al. 2017; Pieczka et al. 2016)
Land atmosphere interactions	Improved understanding of soil moisture feedbacks on precipitation	(Guillod et al. 2014; Guillod et al. 2015) (indirectly, through assimilation of ESA CCI SM into GLEAM)
	Identifying role of soil moisture on temperature variability and heatwaves	(Casagrande et al. 2015; Hirschi et al. 2014; Miralles et al. 2014a)
	Improved modelling of land evaporation	(Martens et al. 2017; Miralles et al. 2014b)
	Impact of soil moisture on dust and aerosols	(Klingmüller et al. 2016)
Global biogeochemical cycles	Benchmarking and calibrating global vegetation models	(Szczypta et al. 2014; Traore et al. 2014)
	Impact of soil moisture dynamics on vegetation productivity	Barichivich et al. (2014); Chen et al. (2014); McNally et al. (2016); Muñoz et al. (2014); Nicolai-Shaw et al. (2016); Papagiannopoulou et al. (2017a); Papagiannopoulou et al. (2017b); Szczypta et al. (2014)
	Connecting trends in soil moisture and vegetation productivity	(Dorigo et al. 2012; Feng 2016)
	Improved crop modelling	(Qiu et al. 2016b; Sakai et al.)

	Assessing drivers of fire activity	(Charles et al. 2016; Forkel et al. 2016)
Hydrology and land surface modelling	Benchmarking model *states* in hydrological and land surface models	(Du et al. 2016; Fang et al. 2016; Lauer et al. 2017; Loew et al. 2013; Schellekens et al. 2017; Spennemann et al. 2015; Szczypta et al. 2014)
	Benchmarking model *processes* in hydrological and land surface models (e.g. dry down)	(Chen et al. 2016)
	Persistence and prediction of soil moisture anomalies in land surface models	(Nicolai-Shaw et al. 2016)
	Improving runoff predictions and flood (risk) modelling	(Massari et al. 2015; Tramblay et al. 2014)
	Improved water budget modelling	(Abera et al. 2016; Allam et al. 2016)
	Assessing irrigation	(Kumar et al. 2015; Qiu et al. 2016b)
	Assessing the impact of agricultural intensification on soil moisture	(Liu et al. 2015)
	Computing cumulative precipitation amounts	(Ciabatta et al. 2016)
Drought applications	Validation of drought indices	(van der Schrier et al. 2013)
	Development of new drought index	(Carrão et al. 2016; Enenkel et al. 2016; Rahmani et al. 2016)
	Improved detection of agricultural droughts	(Liu et al. 2015; Yuan et al. 2015)
	Soil moisture for integrated drought monitoring	(Enenkel et al. 2016; McNally et al. 2016; Nicolai-Shaw et al. 2016; Rahmani et al. 2016)
Meteorological applications	Improving NWP land surface scheme	(Arnault et al., 2015 and Zhan et al., 2016) and see Section **Error! Reference source not found.** of this PUG

4.1 Assessing climate variability and change

As soil moisture is an integrative component of the Earth system, any large scale variability or change in our climate should manifest itself in globally observed patterns. In this role, ESA CCI SM has made a significant contribution to the body of evidence of natural and human-induced climate variability and change. Emblematic for this is the contribution of ESA CCI SM to the

State of the Climate Reports that are issued every year by National Oceanic and Atmospheric Administration (e.g., Blunden and Arndt 2016).

Several studies have shown a clear relationship between major oceanic-atmospheric modes of variability in the climate system, e.g. El Niño Southern Oscillation (ENSO), and variations in ESA CCI SM (Bauer-Marschallinger et al. 2013; Dorigo et al. 2016; Miralles et al. 2014b; Nicolai-Shaw et al. 2016). By applying enhanced statistical methods to the multi-decadal ESA CCI SM v0.1 dataset over Australia, Bauer-Marschallinger et al. (2013) were able to disentangle the portion of soil moisture variability that is driven by the major climate oscillations affecting this continent, i.e., ENSO, the Indian Ocean Dipole and the Antarctic Oscillation, from other modes of short-term and long-term variability. Miralles et al. (2014b) showed that inter-annual soil moisture variability as observed by ESA CCI SM COMBINED v02.2 largely drives the observed large-scale variability in continental evaporation.

ESA CCI SM has been widely used to assess global trends in soil moisture, mostly in combination with LSMs. Based on ESA CCI SM v0.1 (Dorigo et al. 2012) computed that for the period 1988–2010 27% of the area covered by the dataset showed significant trends, of which almost three quarters were drying trends. The strong tendency towards drying were largely confirmed by trends computed for the same period from ERA-Interim and GLDAS-Noah (Dorigo et al. 2012), and ERA-Interim/Land and MERRA-Land (Albergel et al. 2013), although the spatial trend patterns were not everywhere congruent between datasets. The agreement in trends between a newer version of ESA CCI SM (v02.2) and MERRA-Land were recently confirmed by Su et al. (2016). Trend analyses performed on a more regional scale, but for different time periods (An et al. 2016; Qiu et al. 2016b; Rahmani et al. 2016) generally confirmed the results obtained at the global scale while providing a more detailed view on the impact of local land management practices, e.g. irrigation, on observed trends (Qiu et al. 2016b), and the impact of soil moisture trends in regional climate (Klingmüller et al. 2016). Feng (2016) made an assessment of the drivers of trends in ESA CCI SM COMBINED v02.2 soil moisture and concluded that at the global scale climate change is by far the most important driver of changes in soil moisture, although at the regional level vegetation change may play a significant role. Nevertheless, given the limitations in record lengths, the impact of low-frequency climate oscillations on trends should first be carefully addressed before any robust conclusion about the sign and magnitude of the trend can be drawn (Miralles et al. 2014b). Likewise, the potential impact of dataset artefacts should be carefully quantified and corrected for (Su et al. 2016).

4.2 Land-atmosphere interactions

As soil moisture is essential in partitioning the fluxes of water and energy at the land surface, it can affect the dynamics of humidity and temperature in the lower troposphere. This control of soil moisture on evapotranspiration is important for the intensity and persistence of heatwaves, as the depletion of soil moisture and the resulting reduction in evaporative cooling may trigger an amplified increase in air temperature (Fischer et al. 2007b; Hirschi et al. 2011; Miralles et al. 2014a; Seneviratne et al. 2006c). While many studies on soil moisture–evapotranspiration and soil moisture–temperature coupling are based on modelling results or use precipitation-based drought indices as a proxy for soil moisture, ESA CCI SM enables analyses based on long-term soil moisture estimates (Hirschi et al. 2014; Miralles et al. 2014a). The 2003 heatwave in Europe and the 2010 heatwave in Russia both showed distinct negative anomalies in ESA CCI SM v02.1 during the heatwaves, amplifying the lack of evaporative cooling and favouring the progressive build-up of atmospheric heat in the atmospheric boundary layer (Miralles et al. 2014a). Moreover, the temporal evolution and timing of periods of extreme dry soil moisture conditions in ESA CCI SM COMBINED v02.2 coincide well with anomalies in evapotranspiration, temperature, and fAPAR (Nicolai-Shaw et al. 2016).

Limitations with respect to the depth of the soil moisture retrievals (i.e., reporting the content of moisture in the first few centimetres as opposed to the entire root depth affecting transpiration) have triggered some debate about its appropriateness to investigate evapotranspiration dynamics and atmospheric feedbacks (Hirschi et al. 2014). Hirschi et al. (2014) showed that the strength of the relationship between soil moisture and temperature extremes appears underestimated with ESA CCI SM remote sensing-based surface soil moisture compared to estimates based on the Standardized Precipitation Index (SPI; McKee et al. 1993; Stagge et al. 2015). This is related to an underestimation of the temporal dynamics and of large dry/wet anomalies within ESA CCI SM. This effect is enhanced under extreme dry conditions and may lead to a decoupling of the surface layer from deeper layers and from atmospheric fluxes (and resulting temperatures). Thus the added value of root-zone soil moisture is likely more important for applications dealing with extreme conditions, while for mean climatological applications the information content in the surface layer appears adequate. In addition, the importance of having root-zone soil moisture information also seems to depend on the application. For example, (Qiu et al. 2016a) showed that the prediction of near-future vegetation anomalies profits from vertically integrated soil moisture (as an approximation of root-zone soil moisture) as opposed to surface soil moisture alone. In a later study however they found no clear evidence that using vertically extrapolated soil moisture as opposed to surface soil moisture observations enhances the estimation of surface energy fluxes (Qiu et al. 2016a). The assimilation of remote sensing surface soil moisture into a land surface model (e.g., Lannoy and Reichle 2016) provides a possible alternative here. In fact, root zone soil moisture estimates by the satellite-based Global Land Evaporation Amsterdam Model (GLEAM; Miralles et al. 2011) are already improved by the assimilation of ESA CCI SM, while the overall quality of evaporation estimates remains similar after assimilation (Martens et al. 2017). Also, the assimilation of ESA CCI SM COMBINED v02.1

helped interpreting global land evaporation patterns and multi-annual variability in response to the El Niño Southern Oscillation (Miralles et al. 2014b).

Soil moisture also affects precipitation through evapotranspiration. Yet, the effect of soil moisture on precipitation is much more debated than for air temperature. Studies report both positive or negative feedbacks, and even no feedback. Using a precursor of ESA CCI SM, Taylor et al. (2012) identified a spatially negative feedback of soil moisture on convective precipitation regarding the location, i.e., that afternoon rain is more likely over relatively dry soils due to mesoscale circulation effects. Guillod et al. (2015) revisited the soil moisture effect on precipitation using GLEAM root-zone soil moisture with ESA CCI SM COMBINED v02.1 assimilated, and showed that spatial and temporal correlations with opposite signs may coexist within the same region: precipitation events take place preferentially during wet periods (moisture recycling), but within the area have a preference to fall over comparatively drier patches (local, spatially negative feedbacks).

A more indirect but potentially strong soil moisture – atmosphere feedback was found by Klingmüller et al. (2016), who were able to link an observed positive trend in Aerosol Optical Depth (AOD) in the Middle East to a negative trend in ESA CCI SM COMBINED v02.1. As lower soil moisture translates into enhanced dust emissions, their results suggested that increasing temperature and decreasing relative humidity in the last decade have promoted soil drying, leading to increased dust emissions and AOD. These changes in atmospheric composition again may have considerable impact on radiative forcing and precipitation initiation (Ramanathan et al. 2001) and as such impact the energy and water cycles in the area.

4.3 Global biogeochemical cycles

Soil moisture is a regulator for various processes in terrestrial ecosystems such as plant phenology, photosynthesis, biomass allocation, turnover, and mortality; and the accumulation and decomposition of carbon in soils (Carvalhais et al. 2014; Nemani et al. 2003; Reichstein et al. 2013; Richardson et al. 2013). Low soil moisture during drought reduces photosynthesis, enhances ecosystem disturbances such as insect infestations or fires, and thus causes plant mortality and accumulation of dead biomass in litter and soils (Allen et al. 2010; McDowell et al. 2011; Thurner et al. 2016). The release of carbon from soils to the atmosphere through respiration is also controlled by soil moisture (Reichstein and Beer, 2008). Consequently, soil moisture is a strong control on variations in the global carbon cycle (Ahlström et al. 2013; Poulter et al. 2014; van der Molen et al. 2012).

Despite the importance of soil moisture for the global carbon cycle, satellite-derived soil moisture data is currently under-explored in carbon cycle and ecosystem research. Because long-term soil moisture observations were lacking until recently, most studies on the effects of soil moisture on vegetation relied on precipitation estimates (Du et al. 2013; Poulter et al.

2013), indirect drought indices (Hogg et al. 2013; Ji and Peters 2003), or soil moisture estimates from land surface models (Forkel et al. 2015; Rahmani et al. 2016). More recently, authors used ESA CCI SM to assess impacts of water availability and droughts on plant phenology and productivity based on satellite-derived vegetation indices such as the Normalized Difference Vegetation Index (NDVI) or the Leaf Area Index (LAI). For example, Szczypta et al. (2014) used ESA CCI SM v0.1, modelled soil moisture, and LAI over the Euro-Mediterranean zone to evaluate two land surface models and to predict LAI anomalies over cropland. LAI was predictable from ESA CCI SM in large homogeneous cropland regions, e.g. in Southern Russia (Szczypta et al. 2014). Strong positive relationships between ESA CCI SM COMBINED and NDVI were also found for Australia (Chen et al. 2014; v0.1), for croplands in the North China plains (Qiu et al. 2016b; v0.1), and for East Africa (McNally et al. 2016; v02.1). Generally, many regions with positive (greening) or negative (browning) trends in NDVI show also positive and negative trends in ESA CCI SM v0.1, respectively (Dorigo et al. 2012). This co-occurrence of soil moisture and NDVI trends reflects the strong water control on vegetation phenology and productivity. Interestingly, soil moisture from ESA CCI SM v0.1 was also correlated with NDVI in some boreal forests which are primarily temperature-controlled (Barichivich et al. 2014). In these regions, soil moisture and vegetation productivity were controlled by variations in the accumulation and thawing of winter snow packs (Barichivich et al. 2014). However, some water-limited regions had negative EAA CCI SM v0.1 soil moisture trends with no corresponding trend in NDVI (Dorigo et al. 2012). In these cases, the positive relation between surface soil moisture and vegetation is likely modified by vegetation type and vegetation density (Feng, 2016; McNally et al., 2016). For example, densely vegetated areas in East Africa show stronger correlations between ESA CCI SM COMBINED v02.1 soil moisture and NDVI than sparsely vegetated areas (McNally et al., 2016). Novel data-driven approaches allow to assess the share of ESA CCI SM in controlling NDVI variability as opposed to other water and climate drivers (Papagiannopoulou et al. (2017a); Papagiannopoulou et al. (2017b)). **Error! Reference source not found.** shows the correlation between the latest ESA CCI SM COMBINED (v03.2) product and NDVI GIMMS 3G (Tucker et al. 2005) with a lag time of soil moisture preceding NDVI of 16 days. In most regions and especially in water-limited areas such as the Sahel, there is a strong and direct response of NDVI to soil moisture. On the other hand, correlations are negative in many temperate regions. This is likely due to the fact that NDVI is highest in summer months when soil moisture decreases. This demonstrates that vegetation productivity in temperate regions is primarily temperature-controlled and strongly affected by human activities through agriculture or forest management (Forkel et al. (2015); Papagiannopoulou et al. (2017b)).

Apart from the analysis of relations with vegetation indices, the ESA CCI SM datasets have been occasionally used in other ecosystem studies. For example, Muñoz et al. (2014) investigated tree ring chronologies of Conifers in the Andeans in conjunction with soil moisture variability from ESA CCI SM v0.1. The study revealed a previously unobserved relation between tree growth and summer soil moisture (Muñoz et al., 2014). Furthermore, ESA CCI SM v0.1 and vegetation data were used to evaluate ecosystem models (Szczypta et al. 2014; Traore et al. 2014). Thereby, the results of Traore et al. (2014) demonstrate that a model that best performs for soil moisture does not necessarily best perform for plant productivity. This demonstrates the need to jointly use soil moisture and vegetation or carbon cycle observations to improve global ecosystem/carbon cycle models (Kaminski et al. 2013). For example, SMOS soil moisture data and observations of atmospheric CO_2 have been used to estimate parameters of a global vegetation model within a carbon cycle data assimilation system (Scholze et al. 2016). The use of the ESA CCI SM in such an analysis could potentially constrain model uncertainties regarding the long-term hydrological control on vegetation productivity and ecosystem respiration. However, a major source of uncertainty about the future terrestrial carbon cycle is related to how global ecosystem models represent carbon turnover, vegetation dynamics, and disturbances such as fires (Friend et al. 2014). It was previously shown that variations in satellite-derived soil moisture are related to extreme fire events in boreal forests (Bartsch et al. 2009; Forkel et al. 2012). Consequently, the ESA CCI SM COMBINED dataset has been used together with climate, vegetation, and socio-economic data to assess controls on fire activity globally and to identify appropriate structures for global fire models (Charles et al. 2016; Forkel et al. 2016).

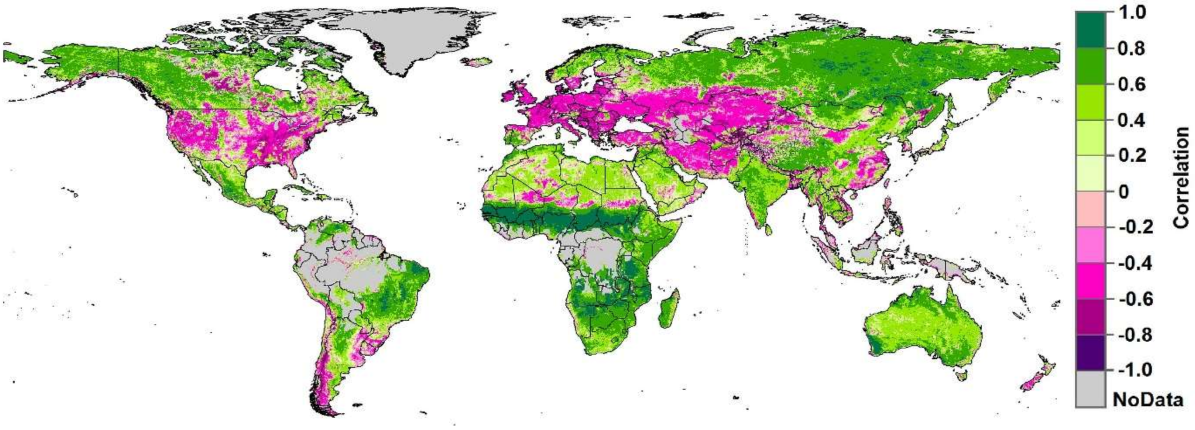

Figure 9: Mean Pearson correlation coefficient R between ESA CCI soil moisture v03.1 and GIMMS NDVI3g for the period 1991 to 2013 for a lag time of soil moisture preceding NDVI by 16 days.

4.4 Hydrological and land surface modelling

As soil moisture drives processes like runoff, flooding, evaporation, infiltration, and ground water recharge, it is important for hydrological models to accurately map soil moisture states. The potential of using ESA CCI SM to validate surface soil moisture fields in state-of-the-art LSMs, reanalysis products, and large-scale hydrological models has been largely recognized (Fang et al. 2016; Loew et al. 2013; Spennemann et al. 2015; Szczypta et al. 2014). Schellekens et al. (2017) exploited the long-term availability of ESA CCI SM COMBINED v02.2 to validate according to a standardised protocol the soil moisture fields of ten global hydrological and land surface models, all forced with the same meteorological forcing dataset for the period 1979-2012. In a similar systematic way, ESA CCI SM COMBINED (v0.1 and v02.2, respectively) was used to evaluate the model outputs of CMIP (Du et al. 2016; Lauer et al. 2017). New insights in the model representation of hydrological processes like infiltration have been offered by comparing the memory length (Chen et al. 2016) and the frequency domains (Polcher et al. 2016) between LSMs and remote sensing products, including ESA CCI SM COMBINED v02.3.

Satellite soil moisture data can bring important benefits in run-off modelling and forecasting both through an improved initialisation of rainfall-runoff models and through data assimilation techniques that allow for updating the soil moisture states. Several studies have shown the positive impact on flood and runoff prediction through assimilation of single sensor soil moisture products, e.g. obtained from ASCAT (Brocca et al. 2010), AMSR-E (Sahoo et al. 2013), and SMOS (Lievens et al. 2015). Wanders et al. (2014) and Alvarez-Garreton et al. (2015) showed the improved skill when jointly assimilating multiple soil moisture products (SMOS, ASCAT and AMSR-E), resulting mainly from improved temporal sampling. Long-term homogeneous soil moisture products like ESA CCI SM become important in flood modelling studies that require a multi-year period for the calibration and validation of model parameters. Assimilating the ESA CCI SM COMBINED v02.2 product over the Upper Niger River basin improved run-off predictions even though the simulation of the rainfall-runoff model was already good (Massari et al. 2015). Tramblay et al. (2014) used the ESA CCI SM product to better constrain model parameters, and hence reduce uncertainties, of a parsimonious hydrological model in the Mono River basin (Africa), with the goal to evaluate the impact of climate change on extreme events. Further studies are clearly needed to assess the full potential of ESA CCI SM product for run-off modelling and forecasting. For example, even a simple model based only on persistence allows for the prediction of soil moisture (Nicolai-Shaw et al. 2016), and exploiting this characteristic could contibute to improved early warning systems.

ESA CCI SM and its Level 2 input products have been used for improving the quantification of the different components of the hydrological cycle, i.e. evaporation (Allam et al. 2016; Martens et al. 2017; Miralles et al. 2014b), groundwater storage (Abelen and Seitz 2013), and rainfall (Ciabatta et al. 2016). Due to its ability to serve as a temporary water reservoir, soil moisture contains information on antecedent precipitation. This principle is being exploited by the SM2RAIN method (Brocca et al. 2014; Brocca et al. 2013), which uses an inversion of the soil-water balance equation to obtain a simple analytical relationship for estimating precipitation accumulations from the knowledge of a soil moisture time-series. The method has been tested on a wide range of Level 2 satellite soil moisture products and ESA CCI SM

COMBINED v02.2 (Brocca et al. 2014; Ciabatta et al. 2016). SM2RAIN realistically reproduces daily precipitation amounts when compared to gauge observations and in certain regions may even perform better than state-of-the-art direct satellite observations of precipitation, even though its performance hinges on the quality of the soil moisture product used as input (Brocca et al. 2014; Ciabatta et al. 2016). Its application to ESA CCI SM COMBINED provides an independent global climatology of precipitation from 1979 onwards. Abera et al. (2016) used the SM2RAIN precipitation product from ESA CCI SM (Ciabatta et al. 2016) to quantify the space-time variability of rainfall, evaporation, runoff and water storage for the Upper Blue Nile river basin in Africa.

ESA CCI SM has also been used to map irrigation, which, is largely unquantified on a global scale and, consequently, not included in most large scale hydrological and/or land surface models (Qiu et al. 2016b). Kumar et al. (2015) used satellite soil moisture observations from ESA CCI SM COMBINED v02.1, ASCAT, AMSR-E, SMOS, and Windsat for the detection of irrigation over United States. By comparing modelled and satellite soil moisture data, irrigated areas can be detected when satellite data and modelled data (the latter do not include irrigation) show different temporal dynamics. Similarly, Qiu et al. (2016b) detected irrigated areas in China by evaluating the differences in trends between ESA CCI SM COMBINED v02.1 and precipitation, and Liu et al. (2015) use ESA CCI SM v0.1 to support the attribution of the aggravating droughts in Northern China to an increase in fertilizer application.

4.5 Drought applications

Soil moisture or agricultural droughts are related to periods of water deficits, and can be driven by a lack of precipitation and/or increased evapotranspiration (Seneviratne et al. 2012). In addition to natural causes, human influences such as poor water management and bad land practices can initiate or exacerbate drought conditions (Liu et al. 2015; Van Loon et al. 2016). Until recently, global soil moisture observations were scarce, which favoured the use of available meteorological observations, such as precipitation and temperature, to develop indices for drought monitoring. Well-known examples, although primarily indicative of meteorological drought rather than soil moisture or agricultural drought, are the SPI and the Palmer Drought Severity Index (PDSI; Palmer 1965).

ESA CCI SM can be used to directly monitor soil moisture or agricultural drought, or help to set up alternative drought indicators. For example, Carrão et al. (2016) and Rahmani et al. (2016) used ESA CCI SM COMBINED (v02.0 and v02.1, respectively) to develop a drought index comparable to SPI but based on actual soil moisture observations instead of precipitation, naming them the Empirical Standardized Soil Moisture Index (ESSMI) and Standardized Soil Moisture Index (SSI), respectively. Carrão et al. (2016) found high correlations between ESSMI and maize, soybean and wheat crop yields in South-Central America and with this index could accurately describe the severe and extreme drought intensities in north-eastern Brazil in 1993, 2012, and 2013. Based on SSI, Rahmani et al. (2016) were able to identify a severe drought event that started in December 2012 in the northern part of the Iran. The Enhanced Combined Drought Index (ECDI) as proposed by Enenkel et al. (2016) combines ESA CCI SM COMBINED v02.2 with satellite-derived observations of rainfall, land surface temperature and vegetation vigour for the detection of drought events, and has been successfully used to detect large-scale drought events in Ethiopia between the years 1992-2014.

McNally et al. (2016) specifically evaluated the use of ESA CCI SM COMBINED v02.2 for agricultural drought and food security monitoring in East Africa, and found that remotely sensed soil moisture is a valuable addition to a 'convergence of evidence' framework for drought monitoring. Like Dorigo et al. (2015b) they emphasize that users should be aware of the spatial and temporal differences in data quality caused for example by significant data gaps prior to 1992, the lack of overlap between sensors, or difficulties with soil moisture retrievals over certain terrains such as heavily vegetated areas. Post 1992 McNally et al. (2016) generally found good agreement between ESA CCI SM and other soil moisture products as well as with NDVI in East Africa. (Yuan et al. 2015) assessed the skill of ESA CCI SM v02.1 in capturing short-term soil moisture droughts over China. They found that the PASSIVE and COMBINED products have better drought detection skills over the sparsely vegetated regions in north-western China while ACTIVE worked best in eastern China. At the global scale Miralles et al. (2014b) identified the effect of El Niño-driven droughts in soil moisture, NDVI and evaporation, using GLEAM and ESA CCI SM COMBINED v02.1. Relationships between extreme dry soil conditions, derived from the ESA CCI SM COMBINED v02.2 dataset, and temperature, precipitation, evapotranspiration and vegetation activity were also found by Nicolai-Shaw et al. (2016). This in combination with the high persistence of soil moisture (Nicolai-Shaw et al. 2016; Seneviratne et al. 2006a) makes the ESA CCI SM dataset valuable for the prediction and monitoring of drought events.

4.6 Meteorological applications

Numerical Weather Prediction (NWP) involves the use of computer models of the Earth system to simulate how the state of the Earth system is likely to evolve over a period of few hours up to 1-2 weeks ahead. It also considers longer timescales (seasonal and climate) through the notion of seamless prediction (Palmer et al. 2008). A number of studies provide strong support for the notion that high skill in short- and medium-range forecasts of air temperature and humidity over land requires proper initialization of soil moisture (Beljaars et al. 1996; Douville et al. 2000; Drusch and Viterbo 2007; van den Hurk et al. 2012). There is evidence also of a similar impact from soil moisture on seasonal forecasts (Koster et al. 2011; Koster et al. 2004b; Weisheimer et al. 2011).

Remotely sensed soil moisture datasets like ESA CCI SM can serve NWP in two ways. First, they can offer a long-term, consistent, and independent reference against which NWP output fields can be evaluated. This may eventually improve meteorological forecasts through a better representation of the land surface, and improved representation of the fluxes between the land surface and the atmosphere in the NWP (see Section **Error! Reference source not found.**). Recently, ECMWF made an offline development in its Land Surface Model HTESSEL (Balsamo et al. 2015; Balsamo et al. 2009), making it possible to add extra layers of soil as well as changing their thickness. An experiment was run which increases the number of soil layers from four to nine and reduces the thickness of the upper soil layer from seven (0-7 cm) to one (0-1) centimetre. One of the rationales for having this thin topsoil layer is having a surface layer that is closer to the depth sampled by existing satellite observations and thus allowing for a better assimilation of these observations. Soil moisture from the first layer of two offline experiments, forced by ERA-Interim reanalysis, and considering either a 1 cm depth (GE8F) or a 7 cm depth (GA89) layer was compared to the ESA CCI SM COMBINED v02.2 over 1979-2014. Correlations were computed for absolute soil moisture and anomaly time series from a 35-day moving average (Dorigo et al. 2015b). We illustrate differences in correlation between the two experiments in **Error! Reference source not found.**. The predominant red colours illustrate that in most areas using a surface layer 1 instead of 7 cm depth leads to a better match with the ESA CCI SM COMBINED dataset. Positive differences frequently reach values higher than 0.2, particularly for correlations on anomaly time series, which shows that a thinner model layer better mimics surface soil moisture variations, as was expected.

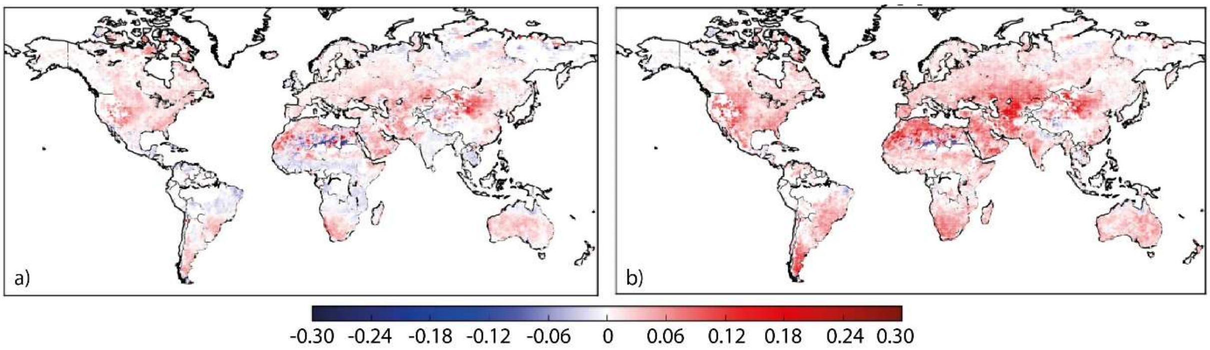

Figure 10 : Differences in correlations of absolute soil moisture values (left) and anomalies (right) differences between ESA CCI SM and soil moisture from the first layer of soil of two offline experiments over 1979-2014. Experiment GE8F has a first layer of soil of 1 cm depth (0-1cm), GA89 of 7 cm depth (0-7cm).

Only few studies have assimilated remotely-sensed soil moisture directly into NWPs and climate models to update their soil moisture fields. Even though this mostly leads to a significant improvement of the model’s soil moisture fields, its impact on the meteorological forecast itself, e.g. on 2 metre air temperature (Bisselink et al. 2011), screen temperature or relative humidity predictions (de Rosnay et al. 2013; Dharssi et al. 2011; Scipal et al. 2008), is typically limited in areas with dense coverage of the ground-based meteorological observing network and difficult to evaluate in poorly observed areas.

5 Specification of the products

5.1 Soil Moisture

The ACTIVE product is the output of merging scatterometer-based soil moisture data, which were derived from AMI-WS and ASCAT. The PASSIVE product merges data from SMMR, SSM/I, TMI, AMSR-E, WindSat, AMSR2, SMOS, SMAP, GPM and FY-3B. The COMBINED is directly generated from the Level 2 products used in both the ACTIVE and PASSIVE products. The data sets have been produced following the method as described by (Gruber et al. 2017; Liu et al. 2011; Wagner 2012). Further information can be found in the ATBD for v06.1 (Scanlon et al., 2021).

The homogenised and merged products provide surface soil moisture with a global coverage and a spatial resolution of 0.25°, and a temporal resolution of 1 day with a reference time at 0:00 UTC. The soil moisture data for the PASSIVE and the COMBINED product are provided in volumetric units [m^3m^{-3}], while the ACTIVE soil moisture data are expressed in percent of saturation [%].

5.2 Product Data Volume

The ESA CCI SM product version v06.1 is provided as global daily images, in NetCDF-4 classic file format and covers the period (yyyy-mm-dd) 1978-11-01 to 2020-12-31 for the PASSIVE and COMBINED products. The ACTIVE product covers the period from 1991-08-05 to 2020-12-31.

Table 3 Temporal coverage and volume size of the products.

Product	Coverage dates	Number of files (days)	Volume size
ACTIVE	19910805 – 20201231	10742	8.3 GB
PASSIVE	19781101 – 20201231	15402	14.1 GB
COMBINED	19781101 – 20201231	15402	16.7 GB
Total	N/A	41546	39.1 GB

5.3 Structure and format of the product

5.3.1 Data file format and file naming

The file format used for storing the data is NetCDF-4 classic. All (NetCDF) files follow the NetCDF Climate and Forecast (CF) Metadata Conventions version 1.7. The NetCDF soil moisture data files are stored in folders for each year with one file per day. The following file naming convention, based on available CCI ECV standards, is applied:

```
ESACCI-<CCI Project>-<Processing Level>-<Data Type>-<Product String>[-<Additional
Segregator>]-<Indicative Date>[<Indicative Time>]-fv<File version>.nc
```

<CCI Project>

Following the file naming convention of CCI data standards working group (DSWG) the name of this project is SOILMOISTURE.

<Processing Level>

The processing level for the ESA CCI SM products is "**L3S**" (super-collated), where observations from multiple instruments are combined into a space-time grid.

<Data Type>

The data type for the ACTIVE product is "**SSMS**" (surface soil moisture degree of saturation absolute), and for the PASSIVE and COMBINED product it is "**SSMV**" (surface soil moisture volumetric absolute).

<Product String>

The product string for the ACTIVE product is defined as "**ACTIVE**", for the PASSIVE product it is "**PASSIVE**", and "**COMBINED**" for the COMBINED product.

<Additional Segregator>

Additional segregator not used and not defined.

<Indicative date and time>

This field indicates the date and time for soil moisture data that are stored in the NetCDF file. The format is YYYYMMDDHHmmSS, where YYYY is the four digit year, MM is the two digit month from 01 to 12, DD is the two digit day of the month from 01 to 31, HH the two digit hour from 00 to 23, mm the two digit minute from 00 to 59, and SS the two digit second from 00 to 59. All times relate to UTC.

fv<file version>

The file version number in form xy.z provides information relating the version of the file format that has been used to provide the product. In the global NetCDF header of each data file the product version number specifies the version of the current product. Since product version 02.1 the file version and the product version number are the same.

5.3.2 NetCDF file structure

5.3.2.1 Global NetCDF Attributes

The Global NetCDF attributes are described in Table 4; where differences exist between the ACTIVE, PASSIVE and COMBINED products, these are noted in the table. Global attributes are provided in the data files for two reasons. The attributes "**title**" and "**product version**" provide the minimum usage information about the data, whilst the remaining attributes starting with the "**summary**" attribute provide product discovery metadata for harvesting into catalogues and data federations.

In general, the Global Attributes will be static and not vary between files for the same product version. Explicitly the following attributes vary for every file within a product: "**tracking id**" and "**filename**".

*Table 4 Global NetCDF Attributes for the ESA CCI SM products. Differences between the ACTIVE, PASSIVE and COMBINED products are noted. * denotes used in the ACTIVE and COMBINED products;† denotes used in the PASSIVE and COMBINED products.*

Global Attribute Name	**Content**
Title	ESA CCI Surface Soil Moisture COMBINED / ACTIVE / PASSIVE Product
institution	Technische Universität Wien (AUT); VanderSat B.V. Harleem (NL)
contact	cci_sm_contact@eodc.eu
source	* WARP 5.5R1.1/AMI-WS/ERS12 Level 2 Soil Moisture; WARP 5.4R1.0/AMI-WS/ERS2 Level 2 Soil Moisture; H115: Metop ASCAT Surface Soil Moisture Climate Data Record v5 12.5 km sampling, DOI: 10.15770/EUM_SAF_H_0006; *H116: Metop ASCAT Surface Soil Moisture Climate Data Record v5 Extension 12.5 km sampling; H115: Metop ASCAT Surface Soil Moisture Climate Data Record v5 12.5 km sampling, DOI: 10.15770/EUM_SAF_H_0006; H116: Metop ASCAT Surface Soil Moisture Climate Data Record v5 Extension 12.5 km sampling; † LPRMv06/SMMR/Nimbus 7 L3 Surface Soil Moisture, Ancillary Params, and quality flags; † LPRMv06/SSMI/F08, F11, F13 DMSP L3 Surface Soil Moisture, Ancillary Params, and quality flags; †LPRMv06/TMI/TRMM L2 Surface Soil Moisture, Ancillary Params, and QC; † LPRMv06/AMSR-E/Aqua L2B Surface Soil Moisture, Ancillary Params, and QC; † LPRMv06/WINDSAT/CORIOLIS L2 Surface Soil Moisture, Ancillary Params, and QC;

Global Attribute Name	Content
	† LPRMv06/AMSR2/GCOM-W1 L3 Surface Soil Moisture, Ancillary Params; † LPRMv06/SMOS/MIRAS L3 Surface Soil Moisture, CATDS Level 3 Brightness Temperatures (L3TB) version 300 RE03 & RE04; † LPRMv06/SMAP_radiometer/SMAP L2 Surface Soil Moisture, Ancillary Params, and QC
platform	†Nimbus 7, †DMSP, †TRMM, †AQUA, †Coriolis, † GCOM-W1, †MIRAS, †SMAP; *ERS-1, *ERS-2, *METOP-A, *METOP-B
sensor	†SMMR, †SSM/I, †TMI, †AMSR-E, †WindSat, †AMSR2, †SMOS, †SMAP_radiometer; *AMI-WS, *ASCAT-A, *ASCAT-B
references	http://www.esa-soilmoisture-cci.org; Dorigo, W.A., Wagner, W., Albergel, C., Albrecht, F., Balsamo, G., Brocca, L., Chung, D., Ertl, M., Forkel, M., Gruber, A., Haas, E., Hamer, D. P. Hirschi, M., Ikonen, J., De Jeu, R. Kidd, R. Lahoz, W., Liu, Y.Y., Miralles, D., Lecomte, P. (2017) ESA CCI Soil Moisture for improved Earth system understanding: State-of-the art and future directions. In Remote Sensing of Environment, 2017, ISSN 0034-4257, https://doi.org/10.1016/j.rse.2017.07.001. Gruber, A., Scanlon, T., van der Schalie, R., Wagner, W., Dorigo, W. (2019) Evolution of the ESA CCI Soil Moisture Climate Data Records and their underlying merging methodology. Earth System Science Data 11, 717-739, https://doi.org/10.5194/essd-11-717-2019. Gruber, A., Dorigo, W. A., Crow, W., Wagner W. (2017). Triple Collocation-Based Merging of Satellite Soil Moisture Retrievals. IEEE Transactions on Geoscience and Remote Sensing. PP. 1-13. https://doi.org/10.1109/TGRS.2017.2734070
product_version	06.1
id	<filename>
tracking_id	<xxxxxxxx-yyyy-zzzz-nnnn-mmmmmmmmmmmm> a UUID (Universal Unique Identifier) value
conventions	CF-1.7
standard_name_vocabulary	NetCDF Climate and Forecast (CF) Metadata Convention
summary	This dataset was produced with funding of the ESA CCI+ Soil Moisture project; ESRIN Contract No: 4000126684/19/I-NB
keywords	Soil Moisture/Water Content
naming_authority	TU Wien

Global Attribute Name	Content
keywords_vocabulary	NASA Global Change Master Directory (GCMD) Science Keywords
cdm_data_type	Grid
comment	This dataset was produced with funding of the ESA CCI+ Soil Moisture project; ESRIN Contract No: 4000126684/19/I-NB
history	< file creation date > - product produced
date_created	<file creation date>
creator_name	Department of Geodesy and Geoinformation, Technical University of Vienna (TU Wien)
creator_url	http://climers.geo.tuwien.ac.at
creator_email	cci_sm_developer@eodc.eu
project	Climate Change Initiative – European Space Agency
license	data use is free and open for all registered users
time_coverage_start	19781101T000000Z (PASSIVE and COMBINED; 19911101T000000Z (ACTIVE)
time_coverage_ed	20201231T235959Z
time_coverage_duration	P41Y
time_coverage_resolution	P1D
geospatial_lat_min	-90.0
geospatial_lat_max	90.0
geospatial_lon_min	-180.0
geospatial_lon_max	180.0
geospatial_vertical_min	0.0
geospatial_vertical_max	0.0
geospatial_lat_units	degrees_north
geospatial_lon_units	degrees_east
geospatial_lat_resolution	0.25 degree
geospatial_lon_resolution	0.25 degree
spatial_resolution	25km

5.3.2.2 NetCDF Data File Variables and Attributes

lon

Table 5 Attribute Table for Variable lon

NetCDF Attribute	Description
standard_name	longitude
units	degrees_east
valid_range	[-180.0, 180.0]
_CoordinateAxisType	Lon

lat

Table 6 Attribute Table for Variable Lat

NetCDF Attribute	Description
standard_name	latitude
units	degrees_north
valid_range	[-90.0, 90.0]
_CoordinateAxisType	Lat

time

Table 7 Attribute Table for Variable time (reference time). The type of this variable is double.

NetCDF Attribute	Description
standard_name	Time
units	days since 1970-01-01 00:00:00 UTC
calendar	Standard
_CoordinateAxisType	Time

sm (ACTIVE product)

Table 8 Attribute Table for Variable sm for the ACTIVE product

NetCDF Attribute	Description
long_name	Percent of Saturation Soil Moisture
units	percent
_CoordinateAxes	lat lon time
_FillValue	-9999.0 (NaN); type: float32 (4 bytes)

sm (PASSIVE and COMBINED product)

Table 9 Attribute Table for Variable sm for the PASSIVE and COMBINED products

NetCDF Attribute	Description
long_name	Volumetric Soil Moisture
units	m^3m^{-3}
_CoordinateAxes	lat lon time
_FillValue	-9999.0 (NaN); type: float32 (4 bytes)

sm_uncertainty (ACTIVE product)

Table 10 Attribute Table for Variable sm_noise

NetCDF Attribute	Description
long_name	Percent of Saturation Soil Moisture Uncertainty
Units	percent
_CoordinateAxes	lat lon time
_FillValue	-9999.0 (NaN); type: float32 (4 bytes)

sm_uncertainty (PASSIVE and COMBINED product)

Table 11 Attribute Table for Variable sm_uncertainty for the PASSIVE and COMBINED products

NetCDF Attribute	Description
long_name	Volumetric Soil Moisture Uncertainty
Units	m3 m-3
_CoordinateAxes	lat lon time
_FillValue	-9999.0 (NaN); type: float32 (4 bytes)

dnflag

Table 12 Attribute Table for Variable dnflag

NetCDF Attribute	Description
long_name	Day / Night Flag
flag_values	[0, 1, 2, 3]
flag_meanings	0 = NaN 1 = day 2 = night 3 = combination of day and night
_CoordinateAxes	lat lon time
_FillValue	0 (NaN); type: signed byte

flag

Table 13 Attribute Table for Variable flag

NetCDF Attribute	Description
long_name	Flag
flag_values	[0, 1, 2, 3, 4, 5, 6, 7, 127]
flag_meanings	0 = no_data_inconsistency_detected 1 = snow_coverage_or_temperature_below_zero 2 = dense_vegetation 3 = combination of flag values 1 and 2 4 = others_no_convergence_in_the_model_thus_no_valid_sm_estimates 5 = combination of flag values 1 and 4 6 = combination of flag value 2 and 4 7 = combination of flag values 1, 2, and 4
_CoordinateAxes	lat lon time
_FillValue	127 (NaN); type: signed byte

freqbandID

Table 14 Attribute Table for Variable freqbandID

<table>
<tr><th>NetCDF Attribute</th><th>Description</th></tr>
<tr><td>long_name</td><td>Frequency Band Identification</td></tr>
<tr><td>flag_values</td><td>[0, 1, 2, 3, 4, 8, 9, 10, 11, 16, 17, 18, 19, 24, 25, 26, 27, 32, 33, 34, 35, 64, 65, 66, 67, 72, 73, 74, 75, 80, 81, 82, 83, 128, 130]</td></tr>
<tr><td>flag_meanings</td><td>
Flag values and their meaning
<table>
<tr><th>Value</th><th>Meaning</th><th>Value</th><th>Meaning</th><th>Value</th><th>Meaning</th></tr>
<tr><td>0</td><td>NaN</td><td>19</td><td>L14+C53+C69</td><td>67</td><td>L14+C53+X107</td></tr>
<tr><td>1</td><td>L14</td><td>24</td><td>C68+C69</td><td>72</td><td>C68+X107</td></tr>
<tr><td>2</td><td>C53</td><td>25</td><td>L14+C68+C69</td><td>73</td><td>L14+C68+X107</td></tr>
<tr><td>3</td><td>L14+C53</td><td>26</td><td>C53+C68+C69</td><td>74</td><td>C53+C68+X107</td></tr>
<tr><td>4</td><td>C66</td><td>27</td><td>L14+C53+C68+C69</td><td>75</td><td>L14+C53+C68+X107</td></tr>
<tr><td>8</td><td>C68</td><td>32</td><td>C73</td><td>80</td><td>C69+X107</td></tr>
<tr><td>9</td><td>L14+C68</td><td>33</td><td>L14+C73</td><td>81</td><td>L14+C69+X107</td></tr>
<tr><td>10</td><td>C53+C68</td><td>34</td><td>C53+C73</td><td>82</td><td>C53+C69+X107</td></tr>
<tr><td>11</td><td>L14+C53+C68</td><td>35</td><td>L14+C53+C73</td><td>83</td><td>L14+C53+C69+X107</td></tr>
<tr><td>16</td><td>C69</td><td>64</td><td>X107</td><td>128</td><td>K194</td></tr>
<tr><td>17</td><td>L14+C69</td><td>65</td><td>L14+X107</td><td>130</td><td>C53+K194</td></tr>
<tr><td>18</td><td>C53+C69</td><td>66</td><td>C53+X107</td><td></td><td></td></tr>
</table>
List of major codes and the corresponding frequency bands
<table>
<tr><th>Binary</th><th>Decimal</th><th>Frequency [GHz]</th><th>BandID</th></tr>
<tr><td>00000000</td><td>0</td><td>NaN</td><td>N/A</td></tr>
<tr><td>00000001</td><td>1</td><td>1.4</td><td>L14</td></tr>
<tr><td>00000010</td><td>2</td><td>5.3 / 5.255</td><td>C53</td></tr>
<tr><td>00000100</td><td>4</td><td>6.6</td><td>C66</td></tr>
<tr><td>00001000</td><td>8</td><td>6.8</td><td>C68</td></tr>
<tr><td>00010000</td><td>16</td><td>6.9 / 6.93</td><td>C69</td></tr>
<tr><td>00100000</td><td>32</td><td>7.3</td><td>C73</td></tr>
<tr><td>01000000</td><td>64</td><td>10.65 / 10.7</td><td>X107</td></tr>
<tr><td>10000000</td><td>128</td><td>19.35 / 19.4</td><td>K194</td></tr>
</table>
Sensors and their operating frequencies:
<table>
<tr><th>Sensor</th><th>Operating Frequency [GHz]</th></tr>
<tr><td>SMMR</td><td>6.6 / 10.7</td></tr>
<tr><td>SSM/I</td><td>19.35</td></tr>
<tr><td>TMI</td><td>10.65</td></tr>
<tr><td>AMSR-E</td><td>6.93 / 10.65</td></tr>
<tr><td>AMSR2</td><td>6.93 / 7.3 / 10.65</td></tr>
<tr><td>WindSat</td><td>6.8 / 10.7</td></tr>
<tr><td>SMOS</td><td>1.4</td></tr>
<tr><td>SMAP</td><td>1.4</td></tr>
<tr><td>AMI-WS</td><td>5.3</td></tr>
<tr><td>ASCAT-A/B</td><td>5.255</td></tr>
</table>
</td></tr>
<tr><td>_CoordinateAxes</td><td>lat lon time</td></tr>
<tr><td>_FillValue</td><td>0 (NaN); type: signed integer</td></tr>
</table>

mode

Table 15 Attribute Table for Variable mode

NetCDF Attribute	Description
long_name	Satellite Mode
flag_values	[0, 1, 2, 3]
flag_meanings	0 = NaN 1 = ascending 2 = descending 3 = combination of ascending and descending
_CoordinateAxes	lat lon time
_FillValue	0 (NaN); type: signed byte

sensor

Table 16 Attribute Table for Variable sensor

<table>
<tr><th>NetCDF Attribute</th><th>Description</th></tr>
<tr><td>long_name</td><td>Sensor</td></tr>
<tr><td>flag_values</td><td>[0, 1, 2, 4, 8, 16, 32, 64, 128, 256, 512, 1024, 4096, 8192]*</td></tr>
<tr><td>flag_meanings</td><td>
<table>
<tr><th>Value</th><th>Sensor Combination</th><th>Value</th><th>Sensor Combination</th></tr>
<tr><td>0</td><td>NaN</td><td>64</td><td>SMOS</td></tr>
<tr><td>1</td><td>SMMR</td><td>128</td><td>AMIWS</td></tr>
<tr><td>2</td><td>SSMI</td><td>256</td><td>ASCATA</td></tr>
<tr><td>4</td><td>TMI</td><td>512</td><td>ASCATB</td></tr>
<tr><td>8</td><td>AMSRE</td><td>1024</td><td>SMAP</td></tr>
<tr><td>16</td><td>WindSat</td><td>4096</td><td>GPM</td></tr>
<tr><td>32</td><td>AMSR2</td><td>8192</td><td>FY-3B</td></tr>
</table>
* Note: All value combinations are provided in the netCDF files.</td></tr>
<tr><td>_CoordinateAxes</td><td>lat lon time</td></tr>
<tr><td>_FillValue</td><td>0 (NaN); type: signed integer</td></tr>
</table>

Table 17 Attribute Table for Variable t0

NetCDF Attribute	Description
long_name	Observation Time Stamp
units	days since 1970-01-01 00:00:00 UTC
valid_range	<individual decimal numbers depending on observation timestamp>

_CoordinateAxes	lat lon time
_FillValue	-9999.0; type: double

5.4 Annotation datasets

The surface soil moisture data (sm) are generated by blending passive and active microwave soil moisture retrievals. The data provided are in percentage of saturation [%] units for the ACTIVE product, and volumetric [m^3m^{-3}] units for the PASSIVE and COMBINED products. Quality Flags and Indicators.

5.4.1 sm_uncertainty

The merging of soil moisture data from different sensors requires a harmonisation of the data. The data need to be brought into a common climatology by running them through several scaling procedures performing the cumulative distribution function (CDF-) matching technique. The provided “sm_uncertainty” parameter represents the error variance of the data sets (in the respective climatology of the dataset), estimated through triple collocation (TC) analysis. In periods where TC cannot be applied, or in cases where the TC-based error variance estimates do not converge, sm_uncertainty is set to NaN. The unit of sm_uncertainty for the ACTIVE product is percentage of saturation [%]. For the PASSIVE and the COMBINED product the unit is volumetric [m^3m^{-3}]. For the ACTIVE and the PASSIVE products, the error variance is directly estimated using TC analysis. For the COMBINED product, these estimates are propagated through the SNR blending model using a standard error propagation scheme.

Table 18 sm_uncertainty data provided in the ESA CCI SM Products

Product	Time Period
ACTIVE	1991-08-05 to 2020-12-31
PASSIVE	1987-07-09 to 2020-12-31
COMBINED	1987-07-09 to 2020-12-31

5.4.2 dnflag

The Day or Night Flag gives information, whether the observation(s) occurred at local day (1) or night (2) time. A value of 3 indicates that the data is a result of merging satellite microwave data observed during day as well as during night time. In cases where the information cannot be determined the value is set to 0 (zero).

5.4.3 flag

Flag values are stored as signed bytes, and the default value (NaN, not a number) is 127. By reading the flag for the surface soil moisture data, the user gets information for that grid point. A “0” (zero) informs that the sm value for that grid point has been checked, but there was no inconsistency found. A “1” denotes, that the soil for that location is covered with snow or the temperature is below zero. Reading a “2” indicates that the observed location is covered by dense vegetation, and a “4” stands for all other cases, e.g. no convergence in the model, thus no valid soil moisture estimates.

5.4.4 freqbandID

The surface soil moisture data has its sources from multiple and different satellite sensors, which operate in various frequencies. The freqbandID values are representing the operating frequencies and comprise the combination of different frequency bands. Table 14 lists these combinations.

5.4.5 mode

The NetCDF variable mode stores the information of the sensor’s orbit direction. Ascending direction are denoted as 1, and descending orbit as 2. In cases where the orbit direction cannot be determined, the NaN value 0 (zero) is used. A value of 3 means that the merged data comprises both ascending and descending satellite modes.

5.4.6 sensor

The values for sensor are stored as signed integer, with NaN as 0 (zero). These values indicate the satellite sensors that have been used for a specific grid point. Valid values range from 1 to 864. Table 16 list all available sensor combinations.

5.4.7 t0

The original observation timestamp is stored within the NetCDF variable t0 (t-naught). Time values coming from two different sensors are averaged. Values of -9999.0 are used as NaN values. t0 data values are stored as number of "days since 1970-01-01 00:00:00 UTC" (see Table 17).

5.4.8 time

The reference timestamp of the day is saved in the "time" variable. The data values for the reference time are stored as number of "days since 1970-01-01 00:00:00 UTC"

5.5 Product Grid and Projection

The grid is a 0.25° x 0.25° longitude-latitude global array of points, based on the World Geodetic System 1984 (WGS 84) reference system. Its dimension is 1440 x 720, where the first dimension, X (longitude) is incrementing most rapidly West (-180°) to East (180°), and the second dimension, Y (latitude) is incrementing South (-90°) to North (90°). Grid edges are at multiple of quarter-degree values (e.g. 90, 89.75, 89.5, 89.25, …), and the grid centers are exactly between two grid edges:

First point centre = (–89.875°S, –179.875°W) = Grid Point Index = 0

Second point centre = (–89.875°S, –179.625°W) = Grid Point Index = 1

1441st point centre = (–89.625°S, –179.875°W) = Grid Point Index = 1440

Last point centre = (89.875°N, 179.875°E) = Grid Point Index = 1036799

In total, there are 1440 x 720 = 1036800 grid points, where 244243 points are land points. Figure 11 shows the land points that are used for the merged product.

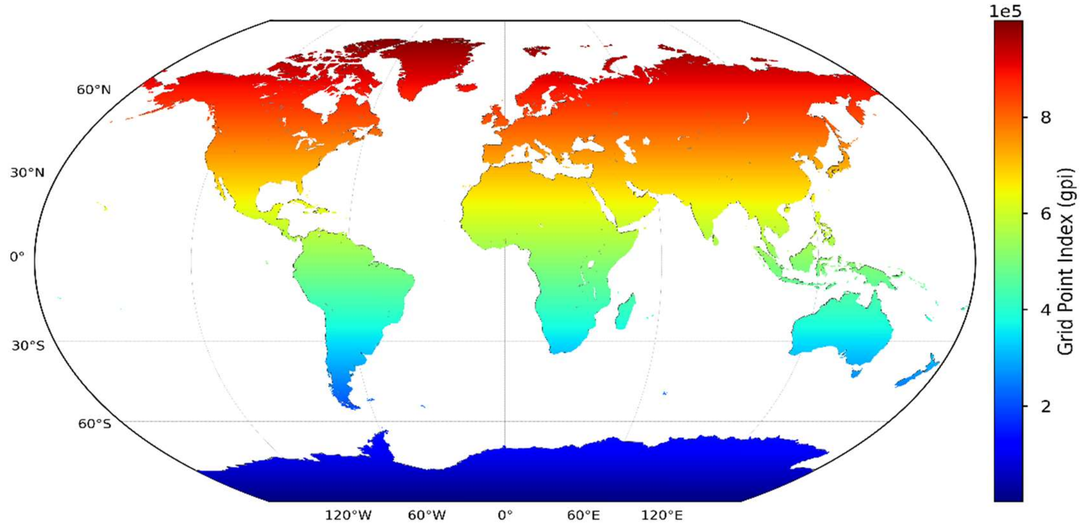

Figure 11: Land mask used for the merged product. The 0.25° grid starts indexing from "lower left" to the "upper right". Note that not every grid points are available for all sensors, e.g. ASCAT retrievals are available between Latitude degrees 80° and –60°.

6 Data Access and Acknowledgements

6.1 Data Access

The ACTIVE, PASSIVE and COMBINED products are freely available for download after the completion of a simple user registration and the approval by the CCI SM team. User registration is available at:

https://climate.esa.int/en/projects/soil-moisture/data/

Registration is required to deter automated systems having direct access to the product. Data downloaded by the registered user can be used by the user and the associated organisation, no onward distribution is permitted.

The current product version is ECV SM v06.1. If you are interested in previous product versions, please search the CEDA archive:

https://catalogue.ceda.ac.uk/

6.2 Data Reader

The esa_cci_sm Python package available on the TU Wien GEO GitHub repository (https://github.com/TUW-GEO/esa_cci_sm) provides readers for the ESA CCI soil moisture datasets (images and time series within the “interface” module). It also allows conversion of daily images to gridded time series via the “reshuffle” module. The README.rst file contains information about installation of the package. Please contact the CCI SM team for advice on using the reader.

6.3 Contact

The CCI SM team can be contact directly via cci_sm_contact@eodc.eu.

E-mails sent to this address reaches both data managers and key project scientists.

6.4 Scientific use only

The ESA CCI SM product is intended for scientific purposes only.

6.5 No onward distribution

Re-export or transfer of the original data (as received from the ECV SM SFTP) by the data users to a third party is prohibited. This is in the best interest of both the individual data providers and the potential users as unrestricted copying of the original data by multiple, independent users may lead to errors in the data.

6.6 Intellectual Property Rights

User acknowledges the respective data owner's full title and ownership of the data and nothing in these terms and conditions shall be construed as granting or implying any rights to, or interest in copyrights or intellectual property rights of the respective data owners.

6.7 Acknowledgement and citation

Whenever the product, made available by the CCI SM project, is used for publication, the data's origin (i.e. the CCI SM project) must be acknowledged and referenced.

The data set should be cited using the complete references as follows:

- Gruber, A. Scanlon, T., van der Schalie, R., Wagner, W., Dorigo, W. (2019) Evolution of the ESA CCI Soil Moisture Climate Data Records and their underlying merging methodology. Earth System Science Data 11, 717-739, https://doi.org/10.5194/essd-11-717-2019
- Gruber, A., Dorigo, W. Crow, W., & Wagner, W. (2017). Triple collocation-based merging of satellite soil moisture retrievals. IEEE Transactions on Geoscience and Remote Sensing, 1-13. https://doi.org/10.1109/TGRS.2017.2734070.
- Dorigo, W.A., Wagner, W., Albergel, C., Albrecht, F., Balsamo, G., Brocca, L., Chung, D., Ertl, M., Forkel, M., Gruber, A., Haas, E., Hamer, P. D., Hirschi, M., Ikonen, J., de Jeu, R., Kidd, R., Lahoz, W., Liu, Y. Y., Miralles, D., Mistelbauer, T., Nicolai-Shaw, N., Parinussa, R., Pratola, C., Reimer, C., van der Schalie, R., Seneviratne, S. I. Smolander, T., Lecomte, P. (2017). ESA CCI Soil Moisture for improved Earth system understanding: State-of-the art and future directions, Remote Sensing of Environment. https://doi.org/10.1016/j.rse.2017.07.001.

6.8 User feedback

Use feedback is warmly welcomed and encouraged. All questions and remarks concerning the product can be addressed to our contact e-mail address provided in Section 6.3.

7 Terminology of Remote Sensing and Earth Observation

Table 19 lists the prime business domain terms from the scientific and technological domains of remote sensing, satellite-based Earth Observation and Soil Moisture retrieval.

Table 19: Business Domain Terminology: Remote Sensing, Earth Observation, Soil Moisture

Term (Acronym)	Description	Synonyms
Remote sensing	Is the acquisition of information about an object or phenomenon without making physical contact with the object. There are two main types of remote sensing: passive remote sensing and active remote sensing, corresponding to active and passive instruments, respectively (see below).	
Sensed object	The object subject of a remote sensing activity.	Sensed target Sensed system
Instrument	In the given context: An imaging microwave instrument flying onboard of an earth observation satellite. The instrument is a payload of the satellite. In a wide sense: Any device that can be used to perform a measurement.	Sensor Measurement device
Active instrument	An instrument that uses its own source of electromagnetic energy for the measurement.	
Scatterometer	An active microwave instrument, measuring the radar backscattering coefficient σ^0 in physical units [dB] or [m^2/m^2].	Radar
Passive instrument	An instrument that measures energy that is reflected or emitted from the sensed object.	
Radiometer	A passive microwave instrument, measuring the brightness temperature T_B in physical unit [K].	
Beam	The direction sensed by single antennae; used to express the fact that a satellite instrument may have several antennas each with its own field of view (FOV).	
Satellite	In the given context always means Earth Observation (EO) satellite.	
Orbit	The path of a satellite on its way around the earth.	
Single overpass Single orbit	The term is used to stress the fact that a satellite instrument scans only once across the earth surface and makes a single or a tuple of measurements per swath node. Implies that individual beams contributing to a measurement result are synchronized to the sensed object.	Single scan

Term (Acronym)	Description	Synonyms
Revisiting orbit	The term is used to stress the fact that measurements of a satellite instrument were not made in a single overpass.	Overlapping orbits Multi-pass orbits
Swath	The area of the earth surface along the ground track of a satellite that is sensed by the instrument in a single overpass; has a definite width but indefinite begin an end; made of an explicit number of nodes in the width-dimension that repeat in regular intervals along the direction of the ground track; each node is the sensed object of a single or a tuple of measurements.	
L<n> Level Processing Level	Processing levels L0 to L4 are an organization of the chain of data processing performed on the payload data from EO satellites.	
Merging	Process of combining the measurements or retrievals from revisiting orbits of a satellite or from many satellites with the aim to reach an improved coverage of the observed domain in space or time. Terms 'merging', 'blending' and 'fusion' appear in the literature sometimes synonymously and sometimes with diversified meanings.	Blending Fusion
Grid	Narrow: A set of nodes, lines or areas in a two-dimensional space that are arranged in a repeated pattern; may result from a construction principle or an actual process that repeats in regular intervals. Wide: Extended to n-dimensional space, and to space-time.	
Node	One point (or area) out of a set of similar points (areas) that together form a grid.	
Grid type	Classification of grids by construction principle.	
Swath grid	The grid originating from a satellite instrument when it senses the individual areas of the earth surface in a repetitive pattern during a single overpass; each grid node represents a single or a tuple of measurements. A swath grid is the result of the projection made by the instrument's beams; images in swath grid are in the perspective of the instrument's point of view (POV). Nodes of revisiting orbits do not coincide, thus swath grids are dynamic and not statically linked to the earth surface.	Data in orbit geometry. Data in instrument projection. Image in the perspective of the instrument's point of view (POV).
Global grid	A spatial grid that is uniformly and statically covering the earth surface. Some global grids use a geoid model (e.g. WGS84 reference ellipsoid) to account for the earth's oblateness. Swath grids can be mapped onto global rids by means of a spatial resampling.	Discrete Global Grid (DGG) (Global) grid system

Term (Acronym)	Description	Synonyms
Global space-time grid	The Cartesian product of a global grid and a timeseries index.	
Geo-referencing	Linkage of grid nodes to points of the earth surface; expressed in latitude and longitude coordinates. Geo-referencing parameters (e.g. satellite ephemeris) allow linking measurement results with the remotely sensed objects on the land surface.	
Time referencing	Linkage of a timeseries index (e.g. swath nodes) to UTC time.	
Measurement	The process of experimentally obtaining one or more quantity values that can reasonably be attributed to a quantity.	Observation
Quantity	A property of a phenomenon, body, or substance, where the property can take on a value that can be expressed as a number and a reference.	Observable Variable
Quantity value	A pair of number and reference, together expressing the value of a quantity.	
Reference	A reference can be a measurement unit, a measurement procedure, a reference material, or a combination of such.	Scale
Measurand	A quantity that is intended to be measured.	
Calibration	An operation performed for an instrument that establishes a relation between measurement standards and the quantity values and uncertainties indicated by the instrument. In case of L1 data, radiometric and geometric calibration coefficients may be either attached (L1a) or applied (L1b).	
Distribution	A function that assigns values to the points of a space, time or space-time domain; the assignment may be continuous or discrete, e.g. to the points of a grid.	
Domain	The range in space, time or space-time that is designated for value assignment.	
Coverage	The fraction of the domain where values have been actually assigned.	
Raster	A two-dimensional array; every element is accessible by the pair of row and column index, is called a pixel, and contains a single or a tuple of values.	Image Raster image
Pixel	An element of a raster.	
Timeseries	A one-dimensional vector; every element is accessible by an index and contains a single or a tuple of values; the index represents points or periods in time that are sampled in equal (or near-equal) intervals.	
Physical system	A part of nature chosen for analysis. The part outside the system is its environment. Effects of the environment on the system are taken into account by an abstraction, and vice-versa. The cut between system and environment is a free choice, generally made to simplify analysis. An isolated system is one which has negligible interaction with its environment.	Geo-physical system

Term (Acronym)	Description	Synonyms
Parameter	A measurable quantity suited to express the state of a physical system. In the given context synonymous for "geophysical parameter".	Sate variable Geophysical parameter Environmental Variable
Local parameter	Characterizes the state of a local and compact object in space (i.e. a local physical system). A Local parameter may be measureable with remote sensing instruments, while others may not be measurable with such instruments, but can still be inferred from direct measurements and additional knowledge about the sensed system (retrieval by an inversion or modelling approach).	Local state variable
Model	A relation between parameters of a physical system, expressed in a mathematical or computable manner. E.g. as an equation system, Y = f(X), where X and Y being tuples of system parameters; or as a computer simulation.	Mathematical model Simulation
Retrieval	The process of obtaining parameter values of a physical system from remote sensing measurements, although the parameters cannot be directly measured (observed) with the used remote sensing instruments. A retrieval is made on a mathematical-physical basis as follows: (1) It is known that at any time quantities X and quantities Y have definite values; (2) it is known that there exists a functional relation between system parameters X and instrument observables Y; (3) there is partial knowledge about the functional relation, e.g. in the form of a forward model Y = f(X) or an inversion X = g(Y); and (4) under certain conditions the knowledge of the functional relation is sufficient to determine X from the measurements of Y.	Parameter retrieval
Retrieval algorithm	The algorithm (or approach, or method) used to retrieve a parameter value from remote sensing measurements.	Retrieval approach or method
Surface Soil Moisture (SSM)	A local geophysical parameter expressing the content of water in the top soil surface layer (of < 2 cm thickness), in physical units [%] or [m^3/m^3]. Typical SSM data products from global satellite observations have a spatial resolution of 25x25 km. Regional products downscaled with use of SAR data are available in a resolution of 1x1 km.	
TUW change detection algorithm	The algorithm used to retrieve the SSM parameter from calibrated measurements of the radar backscattering coefficient σ^0 made by an (active) scatterometer microwave instrument. Uses climate data timeseries of seasonally varying dry and wet reference values. Developed at TUW; implemented by the WARP processing module.	

Term (Acronym)	Description	Synonyms
Land Parameter Retrieval Model (LPRM)	An iterative forward modelling approach used to retrieve the SSM parameter from calibrated measurements of the brightness temperature T_B made by a (passive) radiometer microwave instrument. Uses a global database of physical soil properties. Developed by NASA and VUA.	
Soil Water Index (SWI)	A measure of the profile Soil Moisture content of soil surface layers within 2-100 cm obtained by using an infiltration model (filtering the SSM timeseries with an exponential function).	
Climate	Climate is a measure of the average pattern of variation of meteorological variables (e.g. temperature, humidity, atmospheric pressure, wind, precipitation, atmospheric particle count, etc.) in a given region over long periods of time. A region's climate is generated by the climate system, which has five components: atmosphere, hydrosphere, cryosphere, land surface, and biosphere.	
Essential Climate Variable (ECV)	Essential Climate Variables are geophysical parameters that are required to support the work of the United Nations Framework Convention on Climate Change (UNFCCC), and that are technically and economically feasible for systematic observation. An ECV Data Product combines observations from multiple remote-sensing instruments into a space-time grid; is complete and consistent, with a global and continuing coverage; and is intended for use in climate modeling. Synonyms are Super-collated (L3S) Data and TCDR.	L3S Thematic Climate Data Record (TCDR)
Climatology	Average of a geophysical parameter for a given region; obtained from long-term (many year) observation.	
Seasonality	Seasonal variation of a parameter’s climatology, e.g. variation over the months of a year.	

8 References

Abelen, S., & Seitz, F. (2013). Relating satellite gravimetry data to global soil moisture products via data harmonization and correlation analysis. *Remote Sensing of Environment, 136*, 89-98

Abera, W., Formetta, G., Brocca, L., & Rigon, R. (2016). Water budget modelling of the Upper Blue Nile basin using the JGrass-NewAge model system and satellite data. *Hydrol. Earth Syst. Sci. Discuss., 2016*, 1-28

Ahlström, A., Smith, B., Lindström, J., Rummukainen, M., & Uvo, C.B. (2013). GCM characteristics explain the majority of uncertainty in projected 21st century terrestrial ecosystem carbon balance. *Biogeosciences, 10*, 1517-1528

Albergel, C., Dorigo, W., Reichle, R., Balsamo, G., Rosnay, P.d., Muñoz-Sabater, J., Isaksen, L., Jeu, R.d., & Wagner, W. (2013). Skill and global trend analysis of soil moisture from reanalyses and microwave remote sensing. *Journal Of Hydrometeorology, 14*, 1259–1277

Allam, M.M., Jain Figueroa, A., McLaughlin, D.B., & Eltahir, E.A.B. (2016). Estimation of evaporation over the upper Blue Nile basin by combining observations from satellites and river flow gauges. *Water Resources Research*, n/a-n/a

Allen, C.D., Macalady, A.K., Chenchouni, H., Bachelet, D., McDowell, N., Vennetier, M., Kitzberger, T., Rigling, A., Breshears, D.D., Hogg, E.H., Gonzalez, P., Fensham, R., Zhang, Z., Castro, J., Demidova, N., Lim, J.-H., Allard, G., Running, S.W., Semerci, A., & Cobb, N. (2010). A global overview of drought and heat-induced tree mortality reveals emerging climate change risks for forests. *Forest Ecology and Management, 259*, 660-684

Alvarez-Garreton, C., Ryu, D., Western, A.W., Su, C.H., Crow, W.T., Robertson, D.E., & Leahy, C. (2015). Improving operational flood ensemble prediction by the assimilation of satellite soil moisture: comparison between lumped and semi-distributed schemes. *Hydrol. Earth Syst. Sci., 19*, 1659-1676

An, R., Zhang, L., Wang, Z., Quaye-Ballard, J.A., You, J., Shen, X., Gao, W., Huang, L., Zhao, Y., & Ke, Z. (2016). Validation of the ESA CCI soil moisture product in China. *International Journal of Applied Earth Observation and Geoinformation, 48*, 28-36

Arnault, J., Wagner, S., Rummler, T., Fersch, B., Bliefernicht, J., Andresen, S., Kunstmann, H. (2015). Role of runoff–infiltration partitioning and resolved overland flow on land–atmosphere feedbacks: a case study with the WRF-hydro coupled modeling system for West Africa. J. Hydrometeorol. 17, 1489–1516.

Balsamo, G., Albergel, C., Beljaars, A., Boussetta, S., Brun, E., Cloke, H., Dee, D., Dutra, E., Muñoz-Sabater, J., Pappenberger, F., de Rosnay, P., Stockdale, T., & Vitart, F. (2015). ERA-Interim/Land: a global land surface reanalysis data set. *Hydrol. Earth Syst. Sci., 19*, 389-407

Balsamo, G., Viterbo, P., Beljaars, A., van den Hurk, B., Hirschi, M., Betts, A.K., & Scipal, K. (2009). A Revised Hydrology for the ECMWF Model: Verification from Field Site to Terrestrial Water Storage and Impact in the Integrated Forecast System. *Journal Of Hydrometeorology, 10*, 623-643

Barichivich, J., Briffa, K.R., Myneni, R., Van der Schrier, G., Dorigo, W., Tucker, C.J., Osborn, T., & Melvin, T. (2014). Temperature and Snow-Mediated Moisture Controls of Summer

Photosynthetic Activity in Northern Terrestrial Ecosystems between 1982 and 2011. *Remote Sensing, 6*, 1390-1431

Bartalis, Z. (2009). Spaceborne Scatterometers for Change Detection over Land. In, *Institute for Photogrammetry and Remote Sensing* (p. 148). Vienna: Vienna University of Technology

Bartsch, A., Baltzer, H., & George, C. (2009). The influence of regional surface soil moisture anomalies on forest fires in Siberia observed from satellites. *Environmental Research Letters, 4*, 45021-45021

Bauer-Marschallinger, B., Dorigo, W.A., Wagner, W., & van Dijk, A.I.J.M. (2013). How oceanic oscillation drives soil moisture variations over mainland Australia: An analysis of 32 years of satellite observations. *Journal of Climate, 26*, 10159–10173

Beljaars, A.C.M., Viterbo, P., Miller, M.J., & Betts, A.K. (1996). The Anomalous Rainfall over the United States during July 1993: Sensitivity to Land Surface Parameterization and Soil Moisture Anomalies. *Monthly Weather Review, 124*, 362-383

Bennett , V. and James, S. (2013), ESA, Guidelines for Data Producers - Climate Change Initiative Phase 1, CCI-PRGM-EOPS-TN-13-0009, Issue 1, Revision 1, 24/05/2013

Bisselink, B., Van Meijgaard, E., Dolman, A.J., & De Jeu, R.A.M. (2011). Initializing a regional climate model with satellite-derived soil moisture. *Journal of Geophysical Research D: Atmospheres, 116*

Blunden, J., & Arndt, D.S. (2016). State of the Climate in 2015. *Bulletin of the American Meteorological Society, 97*, S1–S27

Brocca, L., Ciabatta, L., Massari, C., Moramarco, T., Hahn, S., Hasenauer, S., Kidd, R., Dorigo, W., Wagner, W., & Levizzani, V. (2014). Soil as a natural raingauge: estimating global rainfall from satellite soil moisture data. *Journal of Geophysical Research D: Atmospheres, 119*, 5128–5141

Brocca, L., Hasenauer, S., Lacava, T., Melone, F., Moramarco, T., Wagner, W., Dorigo, W., Matgen, P., Martínez-Fernández, J., Llorens, P., Latron, J., Martin, C., & Bittelli, M. (2011). Soil moisture estimation through ASCAT and AMSR-E sensors: An intercomparison and validation study accross Europe. *Remote Sensing of Environment*, submitted

Brocca, L., Melone, F., Moramarco, T., Wagner, W., Naeimi, V., Bartalis, Z., & Hasenauer, S. (2010). Improving runoff prediction through the assimilation of the ASCAT soil moisture product. *Hydrol. Earth Syst. Sci., 14*, 1881-1893

Brocca, L., Moramarco, T., Melone, F., & Wagner, W. (2013). A new method for rainfall estimation through soil moisture observations. *Geophysical Research Letters, 40*, 853-858

Carrão, H., Russo, S., Sepulcre-Canto, G., & Barbosa, P. (2016). An empirical standardized soil moisture index for agricultural drought assessment from remotely sensed data. *International Journal of Applied Earth Observation and Geoinformation, 48*, 74-84

Carvalhais, N., Forkel, M., Khomik, M., Bellarby, J., Jung, M., Migliavacca, M., Mu, M., Saatchi, S., Santoro, M., Thurner, M., Weber, U., Ahrens, B., Beer, C., Cescatti, A., Randerson, J.T., & Reichstein, M. (2014). Global covariation of carbon turnover times with climate in terrestrial ecosystems. *Nature, 514*, 213-217

Casagrande, E., Mueller, B., Miralles, D.G., Entekhabi, D., & Molini, A. (2015). Wavelet correlations to reveal multiscale coupling in geophysical systems. *Journal of Geophysical Research: Atmospheres, 120*, 7555-7572

Charles, I., Luke, T.E., Willmot, K.E., Toshihisa, M., Amin, K.D., Charles, K.G., Jun, W., Eric, M.W., Jejung, L., Jimmy, A., Churchill, O., John, B., Frederick, S.P., & Shahid, H. (2016). Biomass burning, land-cover change, and the hydrological cycle in Northern sub-Saharan Africa. *Environmental Research Letters, 11*, 095005

Chen, T., de Jeu, R.A.M., Liu, Y.Y., van der Werf, G.R., & Dolman, A.J. (2014). Using satellite based soil moisture to quantify the water driven variability in NDVI: A case study over mainland Australia. *Remote Sensing of Environment, 140*, 330-338

Chen, T., McVicar, T., Wang, G., Chen, X., de Jeu, R., Liu, Y., Shen, H., Zhang, F., & Dolman, A. (2016). Advantages of Using Microwave Satellite Soil Moisture over Gridded Precipitation Products and Land Surface Model Output in Assessing Regional Vegetation Water Availability and Growth Dynamics for a Lateral Inflow Receiving Landscape. *Remote Sensing, 8*, 428

Ciabatta, L., Massari, C., Brocca, L., Reimer, C., Hann, S., Paulik, C., Dorigo, W., & Wagner, W. (2016). Using Python® language for the validation of the CCI soil moisture products via SM2RAIN. *PeerJ Preprints, 4*, e2131v2134

De Jeu, R., Dorigo, W., Wagner, W., & Liu, Y. (2011). [Global Climate] Soil Moisture [in: State of the Climate in 2010]. *Bulletin of the American Meteorological Society, 92*, S52-S53

De Jeu, R.A.M., Dorigo, W.A., Parinussa, R.M., Wagner, W., & Chung, D. (2012). [Global Climate] Sol Moisture [in: State of the Climate in 2011]. *Bulletin of the American Meteorological Society, 93*, S30-S34

de Rosnay, P., Drusch, M., Vasiljevic, D., Balsamo, G., Albergel, C., & Isaksen, L. (2013). A simplified Extended Kalman Filter for the global operational soil moisture analysis at ECMWF. *Quarterly Journal of the Royal Meteorological Society, 139*, 1199-1213

Dharssi, I., Bovis, K.J., Macpherson, B., & Jones, C.P. (2011). Operational assimilation of ASCAT surface soil wetness at the Met Office. *Hydrology and Earth System Sciences, 15*, 2729-2746

Diffenbaugh, N.S., Pal, J.S., Giorgi, F., & Gao, X.J. (2007). Heat stress intensification in the Mediterranean climate change hotspot. *Geophysical Research Letters, 34*

Dirmeyer, P.A., Gao, X.A., Zhao, M., Guo, Z.C., Oki, T.K., & Hanasaki, N. (2006). GSWP-2 - Multimodel anlysis and implications for our perception of the land surface. *Bulletin of the American Meteorological Society, 87*, 1381-+

Dorigo, W., Chung, D., Parinussa, R.M., Reimer, C., Hahn, S., Liu, Y.Y., Wagner, W., de Jeu, R.A.M., Paulik, C., & Wang, G. (2014). [Global Climate] Soil Moisture [in: “State of the Climate in 2013”]. *Bulletin American Meteorological Society, 95*, S25-S26

Dorigo, W., & De Jeu, R. (2016). Satellite soil moisture for advancing our understanding of earth system processes and climate change. *International Journal of Applied Earth Observation and Geoinformation, 48*, 1-4

Dorigo, W., De Jeu, R., Chung, D., Parinussa, R., Liu, Y., Wagner, W., & Fernandez-Prieto, D. (2012). Evaluating global trends (1988-2010) in homogenized remotely sensed surface soil moisture. *Geophysical Research Letters, 39*, L18405

Dorigo, W., Reimer, C., Chung, D., Parinussa, R.M., Melzer, T., Wagner, W., de Jeu, R.A.M., & Kidd, R. (2015a). [Hydrological cyce] Soil Moisture [in: "State of the Climate in 2014"]. *Bulletin American Meteorological Society, 96*, S28-S29

Dorigo, W.A., Chung, D., Gruber, A., Hahn, S., Mistelbauer, T., Parinussa, R.M., Paulik, C., Reimer, C., van der Schalie, R., de Jeu, R.A.M., & Wagner, W. (2016). Soil Moisture [in: "State of the Climate in 2015"]. *Bulletin American Meteorological Society, 97*, S31-S32

Dorigo, W.A., Gruber, A., De Jeu, R.A.M., Wagner, W., Stacke, T., Loew, A., Albergel, C., Brocca, L., Chung, D., Parinussa, R.M., & Kidd, R. (2015b). Evaluation of the ESA CCI soil moisture product using ground-based observations. *Remote Sensing of Environment, 162*, 380-395

Dorigo, W., Wagner, W., Albergel, C., Albrecht, F., Balsamo, G., Brocca, L., Chung, D., Ertl, M., Forkel, M., Gruber, A., Haas, E., Hamer, P., Hirschi, M., Ikonen, J., Jeu, R.d., Kidd, R., Lahoz, W., Liu, Y.Y., Miralles, D., Mistelbauer, T., Nicolai-Shaw, N., Parinussa, R., Pratola, C., Reimer, C., Schalie, R.v.d., Seneviratne, S.I., Smolander, T., & Lecomte, P. (2017). ESA CCI Soil Moisture for improved Earth system understanding: state-of-the art and future directions. Remote Sensing of Environment

Douville, H., Viterbo, P., Mahfouf, J.-F., & Beljaars, A.C.M. (2000). Evaluation of the Optimum Interpolation and Nudging Techniques for Soil Moisture Analysis Using FIFE Data. *Monthly Weather Review, 128*, 1733-1756

Drusch, M., & Viterbo, P. (2007). Assimilation of screen-level variables in ECMWF's integrated forecast system: A study on the impact on the forecast quality and analyzed soil moisture. *Monthly Weather Review, 135*, 300-314

Du, E., Vittorio, A.D., & Collins, W.D. (2016). Evaluation of hydrologic components of community land model 4 and bias identification. *International Journal of Applied Earth Observation and Geoinformation, 48*, 5-16

Du, L., Tian, Q., Yu, T., Meng, Q., Jancso, T., Udvardy, P., & Huang, Y. (2013). A comprehensive drought monitoring method integrating MODIS and TRMM data. *International Journal of Applied Earth Observation and Geoinformation, 23*, 245-253

Eaton, B, Gregory, J., Drach, B., Taylor. K., Hankin, S., Blower, J., Caron, J., Signell, R., Bentley, P., Rappa, G., Höck, H., Pamment, A., Juckes, M., Raspaud, M. (2017), NetCDF Climate and Forecast (CF) Metadata Conventions: Version 1.7, 10 August 2017

Enenkel, M., Steiner, C., Mistelbauer, T., Dorigo, W., Wagner, W., See, L., Atzberger, C., Schneider, S., & Rogenhofer, E. (2016). A Combined Satellite-Derived Drought Indicator to Support Humanitarian Aid Organizations. *Remote Sensing, 8*, 340

Entin, J.K., Robock, A., Vinnikov, K.Y., Hollinger, S.E., Liu, S., & Namkhai, A. (2000). Temporal and spatial scales of observed soil moisture variations in the extratropics. *Journal of Geophysical Research, 105*, 11865-11877

Fang, L., Hain, C.R., Zhan, X., & Anderson, M.C. (2016). An inter-comparison of soil moisture data products from satellite remote sensing and a land surface model. *International Journal of Applied Earth Observation and Geoinformation, 48*, 37-50

Feng, H. (2016). Individual contributions of climate and vegetation change to soil moisture trends across multiple spatial scales. *Scientific Reports, 6*, 32782

Findell, K.L., & Eltahir, E.A.B. (2003). Atmospheric controls on soil moisture-boundary layer interactions. Part I: Framework development. *Journal Of Hydrometeorology, 4*, 552-569

Fischer, E.M., Seneviratne, S.I., Luthi, D., & Schar, C. (2007a). Contribution of land-atmosphere coupling to recent European summer heat waves. *Geophysical Research Letters, 34*

Fischer, E.M., Seneviratne, S.I., Vidale, P.L., Luthi, D., & Schar, C. (2007c). Soil moisture - Atmosphere interactions during the 2003 European summer heat wave. *Journal of Climate, 20*, 5081-5099

Forkel, M., Dorigo, W., Lasslop, G., Teubner, I., Chuvieco, E., & Thonicke, K. (2016). Identifying required model structures to predict global fire activity from satellite and climate data. *Geosci. Model Dev. Discuss., 2016*, 1-35

Forkel, M., Migliavacca, M., Thonicke, K., Reichstein, M., Schaphoff, S., Weber, U., & Carvalhais, N. (2015). Co-dominant water control on global inter-annual variability and trends in land surface phenology and greenness. *Global Change Biology*, n/a-n/a

Forkel, M., Thonicke, K., Beer, C., Cramer, W., Bartalev, S., & Schmullius, C. (2012). Extreme fire events are related to previous-year surface moisture conditions in permafrost-underlain larch forests of Siberia. *Environmental Research Letters, 7*, 044021

Friend, A.D., Lucht, W., Rademacher, T.T., Keribin, R., Betts, R., Cadule, P., Ciais, P., Clark, D.B., Dankers, R., Falloon, P.D., Ito, A., Kahana, R., Kleidon, A., Lomas, M.R., Nishina, K., Ostberg, S., Pavlick, R., Peylin, P., Schaphoff, S., Vuichard, N., Warszawski, L., Wiltshire, A., & Woodward, F.I. (2014). Carbon residence time dominates uncertainty in terrestrial vegetation responses to future climate and atmospheric CO2. *Proceedings of the National Academy of Sciences, 111*, 3280-3285

Gruber, A., Dorigo, W., Crow, W., & Wagner, W. (2017). Triple Collocation-Based Merging of Satellite Soil Moisture Retrievals. *IEEE Transactions of Geoscience and Remote Sensing*

Gruber, A., Scanlon, T., van der Schalie, R., Wagner, W., Dorigo, W. (2019) Evolution of the ESA CCI Soil Moisture Climate Data Records and their underlying merging methodology. Earth System Science Data 11, 717-739, https://doi.org/10.5194/essd-11-717-2019

Guillod, B.P., Orlowsky, B., Miralles, D., Teuling, A.J., Blanken, P.D., Buchmann, N., Ciais, P., Ek, M., Findell, K.L., Gentine, P., Lintner, B.R., Scott, R.L., Van den Hurk, B., & I. Seneviratne, S. (2014). Land-surface controls on afternoon precipitation diagnosed from observational data: uncertainties and confounding factors. *Atmos. Chem. Phys., 14*, 8343-8367

Guillod, B.P., Orlowsky, B., Miralles, D.G., Teuling, A.J., & Seneviratne, S.I. (2015). Reconciling spatial and temporal soil moisture effects on afternoon rainfall. *Nature Communications, 6*

Haarsma, R.J., Selten, F., Hurk, B.V., Hazeleger, W., & Wang, X.L. (2009). Drier Mediterranean soils due to greenhouse warming bring easterly winds over summertime central Europe. *Geophysical Research Letters, 36*

Hirschi, M., Mueller, B., Dorigo, W., & Seneviratne, S.I. (2014). Using remotely sensed soil moisture for land–atmosphere coupling diagnostics: The role of surface vs. root-zone soil moisture variability. *Remote Sensing of Environment, 154*, 246-252

Hirschi, M., Seneviratne, S.I., Alexandrov, V., Boberg, F., Boroneant, C., Christensen, O.B., Formayer, H., Orlowsky, B., & Stepanek, P. (2011). Observational evidence for soil-moisture impact on hot extremes in southeastern Europe. *Nature Geoscience, 4*, 17-21

Hogg, E.H., Barr, A.G., & Black, T.A. (2013). A simple soil moisture index for representing multi-year drought impacts on aspen productivity in the western Canadian interior. *Agricultural and Forest Meteorology, 178–179*, 173-182

Holmes, T.R.H., De Jeu, R.A.M., Owe, M., & Dolman, A.J. (2009). Land surface temperature from Ka band (37 GHz) passive microwave observations. *Journal of Geophysical Research-Atmospheres, 114*

HSAF (2018). Algorithm Theoretical Baseline Document (ATBD), Metop ASCAT Soil Moisture Data Records v0.7. In

Ikonen, J., Smolander, T., Pratola, C., Politi, E. (2017), Comprehensive Error Characterisation Report, Version 1.0, 07/07/2017, ESA Climate Change Initiative Phase 2 Soil Moisture Project

Jaeger, E.B., & Seneviratne, S.I. (2011). Impact of soil moisture-atmosphere coupling on European climate extremes and trends in a regional climate model. *Climate Dynamics*, 36, 1919-1939

JCGM (2008). Evaluation of measurement data – Guide to the expression of uncertainty in measurement (GUM). *JCGM*

JCGM (2012). International vocabulary of metrology – Basic and general concepts and assocated terms (VIM). *JCGM*

Ji, L., & Peters, A.J. (2003). Assessing vegetation response to drought in the northern Great Plains using vegetation and drought indices. *Remote Sensing of Environment, 87*, 85-98

Jung, M., Reichstein, M., Ciais, P., Seneviratne, S.I., Sheffield, J., Goulden, M.L., Bonan, G., Cescatti, A., Chen, J., de Jeu, R., Dolman, A.J., Eugster, W., Gerten, D., Gianelle, D., Gobron, N., Heinke, J., Kimball, J., Law, B.E., Montagnani, L., Mu, Q., Mueller, B., Oleson, K., Papale, D., Richardson, A.D., Roupsard, O., Running, S., Tomelleri, E., Viovy, N., Weber, U., Williams, C., Wood, E., Zaehle, S., & Zhang, K. (2010). Recent decline in the global land evapotranspiration trend due to limited moisture supply. *Nature, 467*, 951-954

Kaminski, T., Knorr, W., Schürmann, G., Scholze, M., Rayner, P.J., Zaehle, S., Blessing, S., Dorigo, W., Gayler, V., Giering, R., Gobron, N., Grant, J., Heimann, M., Hooker-Strout, A., Houweling, S., Kato, T., Kattge, J., Kelley, D., Kemp, S., Koffi, E.N., Kostler, C., Mathieu, P.P., Pinty, B., Reick, C., Rödenbeck, C., Schnur, R., Scipal, K., Sebald, C., Stacke, T., Terwisscha van Scheltinga, A., Vossbeck, M., Widmann, H., & Ziehn, T. (2013). The BETHY/JSBACH Carbon Cycle Data Assimilation System: experiences and challenges. *Journal of Geophysical Research: Biogeosciences, 118*, 1414-1426

Kidd, R.A. (2005). Discrete Global Grid Systems. In, *ASCAT Soil Moisture Report Series*: Institute of Photogrammetry and Remote Sensing.

R. Kidd, D. Chung, W. Dorigo, R. De Jeu, (2013) Input/Output Data Definition Document (IODD v2), Version 2.0, 19 December 2013.

R. Kidd, D. Chung, W. Dorigo, R. De Jeu, (2013a), Detailed Processing Model (DPM), Version 2.2, 18 December 2013

Klingmüller, K., Pozzer, A., Metzger, S., Stenchikov, G.L., & Lelieveld, J. (2016). Aerosol optical depth trend over the Middle East. *Atmospheric Chemistry and Physics, 16*, 5063-5073

Koster, R.D., Dirmeyer, P.A., Guo, Z.C., Bonan, G., Chan, E., Cox, P., Gordon, C.T., Kanae, S., Kowalczyk, E., Lawrence, D., Liu, P., Lu, C.H., Malyshev, S., McAvaney, B., Mitchell, K., Mocko, D., Oki, T., Oleson, K., Pitman, A., Sud, Y.C., Taylor, C.M., Verseghy, D., Vasic, R., Xue, Y.K., Yamada, T., & Team, G. (2004a). Regions of strong coupling between soil moisture and precipitation. *Science, 305*, 1138-1140

Koster, R.D., Mahanama, S.P.P., Yamada, T.J., Balsamo, G., Berg, A.A., Boisserie, M., Dirmeyer, P.A., Doblas-Reyes, F.J., Drewitt, G., Gordon, C.T., Guo, Z., Jeong, J.H., Lawrence, D.M., Lee, W.S., Li, Z., Luo, L., Malyshev, S., Merryfield, W.J., Seneviratne, S.I., Stanelle, T., van den Hurk, B., Vitart, F., & Wood, E.F. (2010). Contribution of land surface initialization to subseasonal forecast skill: First results from a multi-model experiment. *Geophysical Research Letters, 37*

Koster, R.D., Mahanama, S.P.P., Yamada, T.J., Balsamo, G., Berg, A.A., Boisserie, M., Dirmeyer, P.A., Doblas-Reyes, F.J., Drewitt, G., Gordon, C.T., Guo, Z., Jeong, J.H., Lee, W.S., Li, Z., Luo, L., Malyshev, S., Merryfield, W.J., Seneviratne, S.I., Stanelle, T., van den Hurk, B.J.J.M., Vitart, F., & Wood, E.F. (2011). The Second Phase of the Global Land–Atmosphere Coupling Experiment: Soil Moisture Contributions to Subseasonal Forecast Skill. *Journal Of Hydrometeorology, 12*, 805-822

Koster, R.D., Suarez, M.J., Liu, P., Jambor, U., Berg, A., Kistler, M., Reichle, R., Rodell, M., & Famiglietti, J. (2004b). Realistic Initialization of Land Surface States: Impacts on Subseasonal Forecast Skill. *Journal Of Hydrometeorology, 5*, 1049-1063

Kumar, S.V., Peters-Lidard, C.D., Santanello, J.A., Reichle, R.H., Draper, C.S., Koster, R.D., Nearing, G., & Jasinski, M.F. (2015). Evaluating the utility of satellite soil moisture retrievals over irrigated areas and the ability of land data assimilation methods to correct for unmodeled processes. *Hydrol. Earth Syst. Sci., 19*, 4463-4478

Lannoy, G.J.M.D., & Reichle, R.H. (2016). Global Assimilation of Multiangle and Multipolarization SMOS Brightness Temperature Observations into the GEOS-5 Catchment Land Surface Model for Soil Moisture Estimation. *Journal Of Hydrometeorology, 17*, 669-691

Lauer, A., Eyring, V., Righi, M., Buchwitz, M., Defourny, P., Evaldsson, M., Friedlingstein, P., de Jeu, R., de Leeuw, G., Loew, A., Merchant, C.J., Müller, B., Popp, T., Reuter, M., Sandven, S., Senftleben, D., Stengel, M., Van Roozendael, M., Wenzel, S., & Willén, U. (2017). Benchmarking CMIP5 models with a subset of ESA CCI Phase 2 data using the ESMValTool. *Remote Sensing of Environment*

Li, L., Njoku, E.G., Im, E., Chang, P.S., & Germain, K.S. (2004). A preliminary survey of radio-frequency interference over the US in Aqua AMSR-E data. *IEEE Transactions on Geoscience and Remote Sensing, 42*, 380-390

Lievens, H., Tomer, S.K., Al Bitar, A., De Lannoy, G.J.M., Drusch, M., Dumedah, G., Hendricks Franssen, H.J., Kerr, Y.H., Martens, B., Pan, M., Roundy, J.K., Vereecken, H., Walker, J.P., Wood, E.F., Verhoest, N.E.C., & Pauwels, V.R.N. (2015). SMOS soil moisture assimilation for improved hydrologic simulation in the Murray Darling Basin, Australia. *Remote Sensing of Environment, 168*, 146-162

Liu, Y., Pan, Z., Zhuang, Q., Miralles, D.G., Teuling, A.J., Zhang, T., An, P., Dong, Z., Zhang, J., He, D., Wang, L., Pan, X., Bai, W., & Niyogi, D. (2015). Agriculture intensifies soil moisture decline in Northern China. *Scientific Reports, 5*, 11261

Liu, Y.Y., Parinussa, R.M., Dorigo, W.A., de Jeu, R.A.M., Wagner, W., van Dijk, A., McCabe, F.M., & Evans, J.P. (2011). Developing an improved soil moisture dataset by blending passive and active microwave satellite-based retrievals. *Hydrology and Earth System Sciences, 15*, 425-436

Liu, Y.Y., Dorigo, W.A., Parinussa, R.M., De Jeu, R.A.M., Wagner, W., McCabe, M.F., Evans, J.P., & Van Dijk, A.I.J.M. (2012). Trend-preserving blending of passive and active microwave soil moisture retrievals. Remote Sensing of Environment, 123, 280-297

Loew, A., Stacke, T., Dorigo, W., de Jeu, R., & Hagemann, S. (2013). Potential and limitations of multidecadal satellite soil moisture observations for selected climate model evaluation studies. *Hydrol. Earth Syst. Sci., 17*, 3523-3542

Mahfouf, J.F. (1991). Analysis of soil moisture from near surface parameters - A feasibility study. *Journal of Applied Meteorology, 30*, 1534-1547

Martens, B., Miralles, D.G., Lievens, H., van der Schalie, R., de Jeu, R.A.M., Fernandez-Prieto, D., Beck, H.E., Dorigo, W.A., & Verhoest, N.E.C. (2017). GLEAM v3: satellite-based land evaporation and root-zone soil moisture. *Geoscientific Model Development, 10*, 1903-1925

Massari, C., Brocca, L., Tarpanelli, A., Ciabatta, L., Camici, S., Moramarco, T., Dorigo, W., & Wagner, W. (2015). Assessing the Potential of CCI Soil Moisture Products for data assimilation in rainfall-runoff modelling: A Case Study for the Niger River. In, *Earth Observation for Water Cycle Science 2015*. Frascati, Italy

McDowell, N.G., Beerling, D.J., Breshears, D.D., Fisher, R.A., Raffa, K.F., & Stitt, M. (2011). The interdependence of mechanisms underlying climate-driven vegetation mortality. *Trends in Ecology & Evolution, 26*, 523-532

McKee, T.B., Doesken, N.J., & Kleist, J. (1993). The Relationship of Drought Frequency and Duration to Time Scales. In, *Eighth Conference on Applied Climatology*. Anaheim, California

McNally, A., Shukla, S., Arsenault, K.R., Wang, S., Peters-Lidard, C.D., & Verdin, J.P. (2016). Evaluating ESA CCI soil moisture in East Africa. *International Journal of Applied Earth Observation and Geoinformation, 48*, 96-109

Miralles, D.G., Holmes, T.R.H., De Jeu, R.A.M., Gash, J.H., Meesters, A.G.C.A., & Dolman, A.J. (2011). Global land-surface evaporation estimated from satellite-based observations. *Hydrology and Earth System Sciences, 15*, 453-469

Miralles, D.G., Teuling, A.J., van Heerwaarden, C.C., & Vila-Guerau de Arellano, J. (2014a). Mega-heatwave temperatures due to combined soil desiccation and atmospheric heat accumulation. *Nature Geosci, 7*, 345-349

Miralles, D.G., Van den Berg, M.J., Gash, J.H., Parinussa, R.M., De Jeu, R.A.M., Beck, H.E., Holmes, D.J., Jimenez, C., Verhoest, N.E.C., Dorigo, W.A., Teuling, A.J., & Dolman, A.J. (2014b). El Niño–La Niña cycle and recent trends in continental evaporation. *Nature Climate Change, 4*, 122-126

Muñoz, A.A., Barichivich, J., Christie, D.A., Dorigo, W., Sauchyn, D., González-Reyes, Á., Villalba, R., Lara, A., Riquelme, N., & González, M.E. (2014). Patterns and drivers of Araucaria araucana forest growth along a biophysical gradient in the northern Patagonian Andes: Linking tree rings with satellite observations of soil moisture. *Austral Ecology, 39*, 158-169

Nemani, R.R., Keeling, C.D., Hashimoto, H., Jolly, W.M., Piper, S.C., Tucker, C.J., Myneni, R.B., & Running, S.W. (2003). Climate-driven increases in global terrestrial net primary production from 1982 to 1999. *Science, 300*, 1560-1563

Nicolai-Shaw, N., Gudmundsson, L., Hirschi, M., & Seneviratne, S.I. (2016). Long-term predictability of soil moisture dynamics at the global scale: Persistence versus large-scale drivers. *Geophysical Research Letters, 43*, 8554-8562

Nijs, A.H.A.d., Parinussa, R.M., Jeu, R.A.M.d., Schellekens, J., & Holmes, T.R.H. (2015). A Methodology to Determine Radio-Frequency Interference in AMSR2 Observations. *IEEE Transactions on Geoscience and Remote Sensing, 53*, 5148-5159

Oki, T., & Kanae, S. (2006). Global hydrological cycles and world water resources. *Science, 313*, 1068-1072

Owe, M., de Jeu, R., & Holmes, T. (2008). Multisensor historical climatology of satellite-derived global land surface moisture. *Journal of Geophysical Research-Earth Surface, 113*, F01002

Owe, M., Jeu, R.d., & Walker, J. (2001). A methodology for surface soil moisture and vegetation optical depth retrieval using the microwave polarization difference index. *IEEE Transactions on Geoscience and Remote Sensing, 39*, 1643-1654

Pal, J.S., & Eltahir, E.A.B. (2003). A feedback mechanism between soil-moisture distribution and storm tracks. *Quarterly Journal of the Royal Meteorological Society, 129*, 2279-2297

Palmer, T.N., Doblas-Reyes, F.J., Weisheimer, A., & Rodwell, M.J. (2008). Toward Seamless Prediction: Calibration of Climate Change Projections Using Seasonal Forecasts. *Bulletin of the American Meteorological Society, 89*, 459-470

Palmer, W.C. (1965). Meteorological drought. *U.S. Weather Bureau Research Paper 45, Washington, DC.*

Papagiannopoulou, C., Miralles, D.G., Decubber, S., Demuzere, M., Verhoest, N.E.C., Dorigo, W.A., & Waegeman, W. (2017a). A non-linear Granger-causality framework to investigate climate–vegetation dynamics. *Geosci. Model Dev., 10*, 1945-1960

Papagiannopoulou, C., Miralles, D.G., Dorigo, W.A., Verhoest, N.E.C., Depoorter, M., & Waegeman, W. (2017b). Vegetation anomalies caused by antecedent precipitation in most of the world. *Environmental Research Letters, 12*, 074016

Parinussa, R.M., De Jeu, R., Wagner, W., Dorigo, W., Fang, F., Teng, W., & Liu, Y.Y. (2013). [Global Climate] Soil Moisture [in: State of the Climate in 2012]. *Bulletin of the American Meteorological Society, 94*, S24-S25

Parinussa, R.M., Holmes, T.R.H., Yilmaz, M.T., & Crow, W.T. (2011). The impact of land surface temperature on soil moisture anomaly detection from passive microwave observations. *Hydrol. Earth Syst. Sci., 15*, 3135-3151

Pieczka, I., Pongrácz, R., Szabóné André, K., Kelemen, F.D., & Bartholy, J. (2016). Sensitivity analysis of different parameterization schemes using RegCM4.3 for the Carpathian region. *Theoretical and Applied Climatology*, 1-14

Polcher, J., Piles, M., Gelati, E., Barella-Ortiz, A., & Tello, M. (2016). Comparing surface-soil moisture from the SMOS mission and the ORCHIDEE land-surface model over the Iberian Peninsula. *Remote Sensing of Environment, 174*, 69-81

Poulter, B., Frank, D., Ciais, P., Myneni, R.B., Andela, N., Bi, J., Broquet, G., Canadell, J.G., Chevallier, F., Liu, Y.Y., Running, S.W., Sitch, S., & van der Werf, G.R. (2014). Contribution of semi-arid ecosystems to interannual variability of the global carbon cycle. *Nature, 509*, 600-603

Poulter, B., Pederson, N., Liu, H., Zhu, Z., D'Arrigo, R., Ciais, P., Davi, N., Frank, D., Leland, C., Myneni, R., Piao, S., & Wang, T. (2013). Recent trends in Inner Asian forest dynamics to temperature and precipitation indicate high sensitivity to climate change. *Agricultural and Forest Meteorology, 178–179*, 31-45

Qiu, J., Crow, W.T., & Nearing, G.S. (2016a). The Impact of Vertical Measurement Depth on the Information Content of Soil Moisture for Latent Heat Flux Estimation. *Journal Of Hydrometeorology, 17*, 2419-2430

Qiu, J., Gao, Q., Wang, S., & Su, Z. (2016b). Comparison of temporal trends from multiple soil moisture data sets and precipitation: The implication of irrigation on regional soil moisture trend. *International Journal of Applied Earth Observation and Geoinformation, 48*, 17-27

Rahmani, A., Golian, S., & Brocca, L. (2016). Multiyear monitoring of soil moisture over Iran through satellite and reanalysis soil moisture products. *International Journal of Applied Earth Observation and Geoinformation, 48*, 85-95

Ramanathan, V., Crutzen, P.J., Kiehl, J.T., & Rosenfeld, D. (2001). Aerosols, Climate, and the Hydrological Cycle. *Science, 294*, 2119-2124

Reichstein, M., Bahn, M., Ciais, P., Frank, D., Mahecha, M.D., Seneviratne, S.I., Zscheischler, J., Beer, C., Buchmann, N., Frank, D.C., Papale, D., Rammig, A., Smith, P., Thonicke, K., van der Velde, M., Vicca, S., Walz, A., & Wattenbach, M. (2013). Climate extremes and the carbon cycle. *Nature, 500*, 287-295

Richardson, A.D., Keenan, T.F., Migliavacca, M., Ryu, Y., Sonnentag, O., & Toomey, M. (2013). Climate change, phenology, and phenological control of vegetation feedbacks to the climate system. *Agricultural and Forest Meteorology, 169*, 156-173

Rowell, D.P., & Jones, R.G. (2006). Causes and uncertainty of future summer drying over Europe. *Climate Dynamics, 27*, 281-299

Sahoo, A.K., De Lannoy, G.J.M., Reichle, R.H., & Houser, P.R. (2013). Assimilation and downscaling of satellite observed soil moisture over the Little River Experimental Watershed in Georgia, USA. *Advances in Water Resources, 52*, 19-33

Sakai, T., Iizumi, T., Okada, M., Nishimori, M., Grünwald, T., Prueger, J., Cescatti, A., Korres, W., Schmidt, M., Carrara, A., Loubet, B., & Ceschia, E. (this issue). Varying applicability of four different satellite-derived soil moisture products to global gridded crop model evaluation. *International Journal of Applied Earth Observation and Geoinformation*

Scanlon, T., Pasik, A., Dorigo, W., de Jeu, R.A.M, Hahn, S. van der Schalie, R., Wagner, W., Kidd, R., Gruber, A., Moesinger, L., Preimesberger, W., Algorithm Theoretical Basis Document (ATBD) supporting product version v06.1, Deliverable 2.1 version 2, 30th March 2021.

Schellekens, J., Dutra, E., Martinez-de la Torre, A., Balsamo, G., van Dijk, A., Weiland, F.S., Minvielle, M., Calvet, J.C., Decharme, B., Eisner, S., Fink, G., Florke, M., Pessenteiner, S., van Beek, R., Polcher, J., Beck, H., Orth, R., Calton, B., Burke, S., Dorigo, W., & Weedon, G.P. (2017). A global water resources ensemble of hydrological models: the eartH2Observe Tier-1 dataset. *Earth System Science Data, 9*, 389-413

Scholze, M., Kaminski, T., Knorr, W., Blessing, S., Vossbeck, M., Grant, J.P., & Scipal, K. (2016). Simultaneous assimilation of SMOS soil moisture and atmospheric CO2 in-situ observations to constrain the global terrestrial carbon cycle. *Remote Sensing of Environment, 180*, 334-345

Schubert, S.D., Suarez, M.J., Pegion, P.J., Koster, R.D., & Bacmeister, J.T. (2004). On the cause of the 1930s Dust Bowl. *Science, 303*, 1855-1859

Scipal, K., Drusch, M., & Wagner, W. (2008). Assimilation of a ERS scatterometer derived soil moisture index in the ECMWF numerical weather prediction system. *Advances in Water Resources, 31*, 1101-1112

Seneviratne, S.I., Corti, T., Davin, E.L., Hirschi, M., Jaeger, E.B., Lehner, I., Orlowsky, B., & Teuling, A.J. (2010). Investigating soil moisture-climate interactions in a changing climate - a review. *Earth-Science Reviews, 99*, 125-161

Seneviratne, S.I., Koster, R.D., Guo, Z., Dirmeyer, P.A., Kowalczyk, E., Lawrence, D., Liu, P., Mocko, D., Lu, C.-H., Oleson, K.W., & Verseghy, D. (2006a). Soil Moisture Memory in AGCM Simulations: Analysis of Global Land–Atmosphere Coupling Experiment (GLACE) Data. *Journal Of Hydrometeorology, 7*, 1090-1112

Seneviratne, S.I., Luthi, D., Litschi, M., & Schar, C. (2006b). Land-atmosphere coupling and climate change in Europe. *Nature, 443*, 205-209

Seneviratne, S.I., Lüthi, D., Litschi, M., & Schär, C. (2006c). Land-atmosphere coupling and climate change in Europe. *Nature, 443*, 205-209

Seneviratne, S.I., Nicholls, N., Easterling, D., Goodess, C.M., Kanae, S., Kossin, J., Luo, Y., Marengo, J., McInnes, K., Rahimi, M., Reichstein, M., Sorteberg, A., Vera, C., & Zhang, X. (2012). Managing the Risks of Extreme Events and Disasters to Advance Climate Change Adaptation. A Special Report of Working Groups I and II of the Intergovernmental Panel on Climate Change. In C.B. Field, V. Barros, T.F. Stocker, D. Qin, D.J. Dokken, K.L. Ebi, M.D. Mastrandrea, K.J. Mach, G.-K. Plattner, S.K. Allen, M. Tignor, and P.M. Midgley (Ed.): Cambridge University Press, Cambridge, UK, and New York, NY, USA, pp. 109-230.

Seto, S., Takahashi, N., & Iguchi, T. (2005). Rain/No-Rain Classification Methods for Microwave Radiometer Observations over Land Using Statistical Information for Brightness Temperatures under No-Rain Conditions. *Journal of Applied Meteorology*

Shukla, J., & Mintz, Y. (1982). Influence of land-surface evapo-transpiration on the earths climate. *Science, 215*, 1498-1501

Spennemann, P.C., Rivera, J.A., Saulo, A.C., & Penalba, O.C. (2015). A Comparison of GLDAS Soil Moisture Anomalies against Standardized Precipitation Index and Multisatellite Estimations over South America. *Journal Of Hydrometeorology, 16*, 158-171

Stagge, J.H., Tallaksen, L.M., Gudmundsson, L., Van Loon, A.F., & Stahl, K. (2015). Candidate Distributions for Climatological Drought Indices (SPI and SPEI). *International Journal of Climatology, 35*, 4027-4040

Su, C.H., Ryu, D., Dorigo, W., Zwieback, S., Gruber, A., Albergel, C., Reichle, R., & Wagner, W. (2016). Homogeneity of a global multi-satellite Climate Data Record on soil moisture. *Geophysical Research Letters, accepted*

Szczypta, C., Calvet, J.C., Maignan, F., Dorigo, W., Baret, F., & Ciais, P. (2014). Suitability of modelled and remotely sensed essential climate variables for monitoring Euro-Mediterranean droughts. *Geosci. Model Dev., 7*, 931-946

Taylor, C.M., De Jeu, R.A.M., Guichard, F., Harris, P.P., & Dorigo, W.A. (2012). Afternoon rain more likely over drier soils. *Nature, 489*, 282–286

Teuling, A.J., Seneviratne, S.I., Stockli, R., Reichstein, M., Moors, E., Ciais, P., Luyssaert, S., van den Hurk, B., Ammann, C., Bernhofer, C., Dellwik, E., Gianelle, D., Gielen, B., Grunwald, T., Klumpp, K., Montagnani, L., Moureaux, C., Sottocornola, M., & Wohlfahrt, G. (2010). Contrasting response of European forest and grassland energy exchange to heatwaves. *Nature Geoscience, 3*, 722-727

Thurner, M., Beer, C., Carvalhais, N., Forkel, M., Santoro, M., Tum, M., & Schmullius, C. (2016). Large-scale variation in boreal and temperate forest carbon turnover rate is related to climate. *Geophysical Research Letters*

Tramblay, Y., Amoussou, E., Dorigo, W., & Mahé, G. (2014). Flood risk under future climate in data sparse regions: linking extreme value models and flood generating processes. *Journal of Hydrology, 519*, 549-558

Traore, A.K., Ciais, P., Vuichard, N., Poulter, B., Viovy, N., Guimberteau, M., Jung, M., Myneni, R., & Fisher, J.B. (2014). Evaluation of the ORCHIDEE ecosystem model over Africa against 25 years of satellite-based water and carbon measurements. *Journal of Geophysical Research: Biogeosciences, 119*, 2014JG002638

Tucker, C.J., Pinzon, J.E., Brown, M.E., Slayback, D.A., Pak, E.W., Mahoney, R., Vermote, E.F., & El Saleous, N. (2005). An extended AVHRR 8-km NDVI dataset compatible with MODIS and SPOT vegetation NDVI data. *International Journal of Remote Sensing, 26*, 4485-4498

van den Hurk, B., Doblas-Reyes, F., Balsamo, G., Koster, R.D., Seneviratne, S.I., & Camargo, H. (2012). Soil moisture effects on seasonal temperature and precipitation forecast scores in Europe. *Climate Dynamics, 38*, 349-362

van der Molen, M.K., Dolman, A.J., Ciais, P., Eglin, T., Gobron, N., Law, B.E., Meir, P., Peters, W., Phillips, O.L., Reichstein, M., Chen, T., Dekker, S.C., Doubková, M., Friedl, M.A., Jung, M., van den Hurk, B.J.J.M., de Jeu, R.A.M., Kruijt, B., Ohta, T., Rebel, K.T., Plummer, S., Seneviratne, S.I., Sitch, S., Teuling, A.J., van der Werf, G.R., & Wang, G. (2012). Drought and ecosystem carbon cycling. *Agricultural and Forest Meteorology, 151*, 765-773

van der Schalie, R., De Jeu, R., Rodriguez-Fernandez, N., Al-Yaari, A., Kerr, Y., Wigneron, J.-P., Parinussa, R., & Drusch, M. (2018). The Effect of Three Different Data Fusion Approaches on the Quality of Soil Moisture Retrievals from Multiple Passive Microwave Sensors. *Remote Sensing* van der Schrier, G., Barichivich, J., Briffa, K.R., & Jones, P.D. (2013). A scPDSI-based global data set of dry and wet spells for 1901–2009. *Journal of Geophysical Research: Atmospheres, 118*, 4025-4048

Van Loon, A.F., Stahl, K., Di Baldassarre, G., Clark, J., Rangecroft, S., Wanders, N., Gleeson, T., Van Dijk, A.I.J.M., Tallaksen, L.M., Hannaford, J., Uijlenhoet, R., Teuling, A.J., Hannah, D.M., Sheffield, J., Svoboda, M., Verbeiren, B., Wagener, T., & Van Lanen, H.A.J. (2016). Drought in a human-modified world: reframing drought definitions, understanding, and analysis approaches. *Hydrol. Earth Syst. Sci., 20*, 3631-3650

Vinnikov, K.Y., Robock, A., Speranskaya, N.A., & Schlosser, C.A. (1996). Scales of temporal and spatial variability of mitlatitude soil moisture. *J. Geophys. Res., 101*, 7163-7174

Wagner, W., W. Dorigo, R. de Jeu, D. Fernandez-Prieto, J. Benveniste, E. Haas, & Ertl, M. (2012). Fusion of active and passive microwave observations to create an Essential Climate Variable data record on soil moisture. In, *XXII ISPRS Congress*. Melbourne,Australia

Wanders, N., Karssenberg, D., de Roo, A., de Jong, S.M., & Bierkens, M.F.P. (2014). The suitability of remotely sensed soil moisture for improving operational flood forecasting. *Hydrol. Earth Syst. Sci., 18*, 2343-2357

Weisheimer, A., Doblas-Reyes, F.J., Jung, T., & Palmer, T.N. (2011). On the predictability of the extreme summer 2003 over Europe. *Geophysical Research Letters, 38*, n/a-n/a

Wu, W.R., & Dickinson, R.E. (2004). Time scales of layered soil moisture memory in the context of land-atmosphere interaction. *Journal of Climate, 17*, 2752-2764

Yuan, X., Ma, Z., Pan, M., & Shi, C. (2015). Microwave remote sensing of short-term droughts during crop growing seasons. *Geophysical Research Letters*, 2015GL064125

Zaitchik, B.F., Macalady, A.K., Bonneau, L.R., & Smith, R.B. (2006). Europe's 2003 heat wave: A satellite view of impacts and land-atmosphere feedbacks. *International Journal of Climatology, 26*, 743-769

Zhan, X., Zheng, W., Fang, L., Liu, J., Hain, C., Yin, J., Ek, M., 2016. A preliminary assessment of the impact of SMAP Soil Moisture on numerical weather Forecasts from GFS and NUWRF models. 2016 IEEE International Geoscience and Remote Sensing Symposium (IGARSS), pp. 5229–5232